choice when detection of structural variants or mutations in noncoding regions represents an important element of investigation. In the long term, considering that costs associated with massively parallel sequencing technology is expected to fall further and that analysis pipelines continue to evolve, it is probable that WGS would be just as workable economically and physically as WES. Limitations of WGS include the requirement of high-quality DNA to explore the full leverage of the mate-pair mapping and the lack of reliable pipelines to detect SVs ranging in size from 50 to a few hundred base pairs. Unexpectedly, the difficulty accompanied by handling the large amount of data produced by WGS was not a significant obstacle, given the power of desktop computers presently available on the market. Whereas samples with suitable quality could be obtained through careful preparation of fresh DNA samples, under detection of SVs may be a more problematic issue to solve. This occurs because current mapping is based on two steps: mapping of the short reads aimed at detecting variations between 1 and 50 bp and mate-pair mapping for detection of SVs larger than a few hundred bases; to our knowledge, a solution that could fill the gap between these two mapping approaches remains to be found.

In conclusion, in this study we identified clear-cut causative mutations among the overwhelming number of DNA variants present in the human genome, in single patients from genetically diverse populations. This happened without ambiguities in a highly heterogeneous disease, ARRP, and in more than 50% of the individuals analyzed. Furthermore, two cases presented mutations involving noncoding parts of the genome. Considering that the majority of patients referred for molecular genetics diagnosis are isolated individuals, our results are relevant not only to basic research, but also to future clinical genetic testing.

Methods

Our research protocol involving humans and animals was approved by the institutional review boards of our respective universities and organizations. Written informed consent for providing medical information and blood samples was obtained from each patient. Experimental procedures are described in detail in *SI Appendix, Methods*.

ACKNOWLEDGMENTS. We thank Anna M. Siemiatkowska and Frans P. M. Cremers for sharing material from a person with RP, Adriana Ransijn for technical help, as well as Andrea Superti-Furga, and Luisa Bonafé for fruitful suggestions. Data storage was ensured by the Vital-IT Center for high-performance computing of the Swiss Institute of Bioinformatics. This work was supported by the Swiss National Science Foundation (Grant 310030_138346) and the Gebert Rüf Foundation, Switzerland (Rare Diseases-New Technologies Grant) (both to C.R.); a Center Grant from the Foundation Fighting Blindness (to E.L.B.); National Institutes of Health Grants DK072301 and MH-084018 (to N.K.); Ministry of Health, Labor and Welfare (MHLW) of Japan [Grant 23300101 (to S.I. and N. Matsumoto) and Grant 23300201 (to S.I.)]; MHLW, the Japan Science and Technology Agency, and the Strategic Research Program for Brain Sciences (N. Matsumoto); and a Grant-in-Aid for Scientific Research on Innovative Areas (transcription cycle) from the Ministry of Education, Culture, Sports, Science and Technology of Japan and the Takeda Science Foundation (to N. Matsumoto).

1. Maguire AM, et al. (2008) Safety and efficacy of gene transfer for Leber's congenital amaurosis. *N Engl J Med* 358(21):2240–2248.
2. Bainbridge JW, et al. (2008) Effect of gene therapy on visual function in Leber's congenital amaurosis. *N Engl J Med* 358(21):2231–2239.
3. Cideciyan AV, et al. (2008) Human gene therapy for RPE65 isomerase deficiency activates the retinoid cycle of vision but with slow rod kinetics. *Proc Natl Acad Sci USA* 105(39):15112–15117.
4. Berson EL (1993) Retinitis pigmentosa. The Friedenwald Lecture. *Invest Ophthalmol Vis Sci* 34(5):1659–1676.
5. Berson EL, Rosner B, Sandberg MA, Weigel-DiFranco C, Willett WC (2012) ω-3 intake and visual acuity in patients with retinitis pigmentosa receiving vitamin A. *Arch Ophthalmol* 130(6):707–711.
6. Berson EL, et al. (1993) A randomized trial of vitamin A and vitamin E supplementation for retinitis pigmentosa. *Arch Ophthalmol* 111(6):761–772.
7. Hartong DT, Berson EL, Dryja TP (2006) Retinitis pigmentosa. *Lancet* 368(9549): 1795–1809.
8. Jin ZB, et al. (2008) Identifying pathogenic genetic background of simplex or multiplex retinitis pigmentosa patients: A large scale mutation screening study. *J Med Genet* 45(7):465–472.
9. Tucker T, Marra M, Friedman JM (2009) Massively parallel sequencing: The next big thing in genetic medicine. *Am J Hum Genet* 85(2):142–154.
10. Tuson M, Marfany G, Gonzàlez-Duarte R (2004) Mutation of CERKL, a novel human ceramide kinase gene, causes autosomal recessive retinitis pigmentosa (RP26). *Am J Hum Genet* 74(1):128–138.
11. Aldahmesh MA, et al. (2009) Molecular characterization of retinitis pigmentosa in Saudi Arabia. *Mol Vis* 15:2464–2469.
12. Vervoort R, et al. (2000) Mutational hot spot within a new RPGR exon in X-linked retinitis pigmentosa. *Nat Genet* 25(4):462–466.
13. Sanuki R, et al. (2011) miR-124a is required for hippocampal axogenesis and retinal cone survival through Lhx2 suppression. *Nat Neurosci* 14(9):1125–1134.
14. Cottet S, Schorderet DF (2009) Mechanisms of apoptosis in retinitis pigmentosa. *Curr Mol Med* 9(3):375–383.
15. Rabbani B, Mahdieh N, Hosomichi K, Nakaoka H, Inoue I (2012) Next-generation sequencing: Impact of exome sequencing in characterizing Mendelian disorders. *J Hum Genet* 57(10):621–632.
16. Hosono K, et al. (2012) Two novel mutations in the EYS gene are possible major causes of autosomal recessive retinitis pigmentosa in the Japanese population. *PLoS ONE* 7(2):e31036.
17. Pieras JI, et al. (2011) Copy-number variations in EYS: A significant event in the appearance of arRP. *Invest Ophthalmol Vis Sci* 52(8):5625–5631.
18. van Wijk E, et al. (2006) The DFNB31 gene product whirlin connects to the Usher protein network in the cochlea and retina by direct association with USH2A and VLGR1. *Hum Mol Genet* 15(5):751–765.
19. Rivolta C, Sweklo EA, Berson EL, Dryja TP (2000) Missense mutation in the USH2A gene: Association with recessive retinitis pigmentosa without hearing loss. *Am J Hum Genet* 66(6):1975–1978.
20. Ebermann I, et al. (2007) A novel gene for Usher syndrome type 2: Mutations in the long isoform of whirlin are associated with retinitis pigmentosa and sensorineural hearing loss. *Hum Genet* 121(2):203–211.
21. Yang J, et al. (2010) Ablation of whirlin long isoform disrupts the USH2 protein complex and causes vision and hearing loss. *PLoS Genet* 6(5):e1000955.
22. McLaughlin ME, Sandberg MA, Berson EL, Dryja TP (1993) Recessive mutations in the gene encoding the beta-subunit of rod phosphodiesterase in patients with retinitis pigmentosa. *Nat Genet* 4(2):130–134.
23. Rivolta C, Sharon D, DeAngelis MM, Dryja TP (2002) Retinitis pigmentosa and allied diseases: Numerous diseases, genes, and inheritance patterns. *Hum Mol Genet* 11(10): 1219–1227.
24. Nishiguchi KM, Rivolta C (2012) Genes associated with retinitis pigmentosa and allied diseases are frequently mutated in the general population. *PLoS ONE* 7(7):e41902.
25. Fry AM, Meraldi P, Nigg EA (1998) A centrosomal function for the human Nek2 protein kinase, a member of the NIMA family of cell cycle regulators. *EMBO J* 17(2): 470–481.
26. Quarmby LM, Mahjoub MR (2005) Caught Nek-ing: Cilia and centrioles. *J Cell Sci* 118(Pt 22):5161–5169.
27. Fakhro KA, et al. (2011) Rare copy number variations in congenital heart disease patients identify unique genes in left-right patterning. *Proc Natl Acad Sci USA* 108(7): 2915–2920.
28. Bahe S, Stierhof YD, Wilkinson CJ, Leiss F, Nigg EA (2005) Rootletin forms centriole-associated filaments and functions in centrosome cohesion. *J Cell Biol* 171(1):27–33.
29. Yang J, et al. (2002) Rootletin, a novel coiled-coil protein, is a structural component of the ciliary rootlet. *J Cell Biol* 159(3):431–440.
30. Hollingsworth TJ, Gross AK (2012) Defective trafficking of rhodopsin and its role in retinal degenerations. *Int Rev Cell Mol Biol* 293:1–44.
31. Luo N, Lu J, Sun Y (2012) Evidence of a role of inositol polyphosphate 5-phosphatase INPP5E in cilia formation in zebrafish. *Vision Res* 75:98–107.
32. Patil SB, Hurd TW, Ghosh AK, Murga-Zamalloa CA, Khanna H (2011) Functional analysis of retinitis pigmentosa 2 (RP2) protein reveals variable pathogenic potential of disease-associated missense variants. *PLoS ONE* 6(6):e21379.
33. Chang GQ, Hao Y, Wong F (1993) Apoptosis: Final common pathway of photoreceptor death in rd, rds, and rhodopsin mutant mice. *Neuron* 11(4):595–605.
34. Davis EE, Katsanis N (2012) The ciliopathies: A transitional model into systems biology of human genetic disease. *Curr Opin Genet Dev* 22(3):290–303.
35. Fahim AT, et al. (2011) Allelic heterogeneity and genetic modifier loci contribute to clinical variation in males with X-linked retinitis pigmentosa due to RPGR mutations. *PLoS ONE* 6(8):e23021.

ARTICLE

De Novo Mutations in *GNAO1*, Encoding a $G\alpha_o$ Subunit of Heterotrimeric G Proteins, Cause Epileptic Encephalopathy

Kazuyuki Nakamura,[1,2,9] Hirofumi Kodera,[1,9] Tenpei Akita,[3,9] Masaaki Shiina,[4] Mitsuhiro Kato,[2] Hideki Hoshino,[5] Hiroshi Terashima,[5] Hitoshi Osaka,[6] Shinichi Nakamura,[7] Jun Tohyama,[8] Tatsuro Kumada,[3] Tomonori Furukawa,[3] Satomi Iwata,[3] Takashi Shiihara,[2,10] Masaya Kubota,[5] Satoko Miyatake,[1] Eriko Koshimizu,[1] Kiyomi Nishiyama,[1] Mitsuko Nakashima,[1] Yoshinori Tsurusaki,[1] Noriko Miyake,[1] Kiyoshi Hayasaka,[2] Kazuhiro Ogata,[4] Atsuo Fukuda,[3] Naomichi Matsumoto,[1,*] and Hirotomo Saitsu[1,*]

Heterotrimeric G proteins, composed of α, β, and γ subunits, can transduce a variety of signals from seven-transmembrane-type receptors to intracellular effectors. By whole-exome sequencing and subsequent mutation screening, we identified de novo heterozygous mutations in *GNAO1*, which encodes a $G\alpha_o$ subunit of heterotrimeric G proteins, in four individuals with epileptic encephalopathy. Two of the affected individuals also showed involuntary movements. Somatic mosaicism (approximately 35% to 50% of cells, distributed across multiple cell types, harbored the mutation) was shown in one individual. By mapping the mutation onto three-dimensional models of the Gα subunit in three different complexed states, we found that the three mutants (c.521A>G [p.Asp174Gly], c.836T>A [p.Ile279Asn], and c.572_592del [p.Thr191_Phe197del]) are predicted to destabilize the Gα subunit fold. A fourth mutant (c.607G>A), in which the Gly203 residue located within the highly conserved switch II region is substituted to Arg, is predicted to impair GTP binding and/or activation of downstream effectors, although the p.Gly203Arg substitution might not interfere with Gα binding to G-protein-coupled receptors. Transient-expression experiments suggested that localization to the plasma membrane was variably impaired in the three putatively destabilized mutants. Electrophysiological analysis showed that $G\alpha_o$-mediated inhibition of calcium currents by norepinephrine tended to be lower in three of the four $G\alpha_o$ mutants. These data suggest that aberrant $G\alpha_o$ signaling can cause multiple neurodevelopmental phenotypes, including epileptic encephalopathy and involuntary movements.

Introduction

Epileptic encephalopathy is a group of neurological disorders characterized by severe and progressive cognitive and behavioral impairments, which are most likely caused or made worse by epileptic activity.[1] Ohtahara syndrome (OS [MIM 308350 and 612164]) is the most severe and the earliest form of epileptic encephalopathy and is characterized by tonic spasms mainly in the neonatal period, seizure intractability, and a suppression-burst pattern on electroencephalography (EEG).[2] De novo mutations in three genes, *ARX* (MIM 300382), *STXBP1* (MIM 602926), and *KCNQ2* (MIM 602235), have been reported in individuals with OS.[3–6]

Heterotrimeric guanine-binding proteins (G proteins) are composed of α, β, and γ subunits. In its basal state, Gα is bound with guanosine diphosphate (GDP) and forms the Gαβγ complex. When a seven-transmembrane-type receptor binds its agonist, it activates G proteins by catalyzing the exchange of GDP for guanosine triphosphate (GTP) on the Gα subunit. Subsequently, GTP-bound Gα dissociates from Gβγ, and each of the two complexes activates distinct downstream effectors.[7] In mammals, Gα subunits are divided into four classes: $G\alpha_{i/o}$, $G\alpha_{q/11}$, $G\alpha_s$, and $G\alpha_{12/13}$.[7] $G\alpha_o$, encoded by *GNAO1* (MIM 139311), is extremely abundant in brain tissue, where it can constitute up to approximately 0.5% of membrane protein,[8] suggesting important roles in brain function. In fact, mice lacking $G\alpha_o$ show multiple neurological abnormalities, including generalized tremor, occasional seizures, severe motor-control impairment, hyperalgesia, and behavioral abnormalities with early postnatal lethality.[9,10]

In this study, de novo *GNAO1* mutations were identified in four epileptic-encephalopathy-affected individuals, three of whom were diagnosed with OS. In addition, two of the four individuals showed involuntary movements, suggesting that aberration of $G\alpha_o$ can cause multiple neurodevelopmental phenotypes.

[1]Department of Human Genetics, Yokohama City University Graduate School of Medicine, 3-9 Fukuura, Kanazawa-ku, Yokohama 236-0004, Japan; [2]Department of Pediatrics, Yamagata University Faculty of Medicine, 2-2-2 Iida-nishi, Yamagata 990-9585, Japan; [3]Department of Neurophysiology, Hamamatsu University School of Medicine, 1-20-1 Handayama, Higashi-ku, Hamamatsu 431-3192, Japan; [4]Department of Biochemistry, Yokohama City University Graduate School of Medicine, 3-9 Fukuura, Kanazawa-ku, Yokohama 236-0004, Japan; [5]Division of Neurology, National Center for Child Health and Development, 2-10-1 Okura, Setagaya-ku, Tokyo 157-8535, Japan; [6]Division of Neurology, Clinical Research Institute, Kanagawa Children's Medical Center, 2-138-4 Mutsukawa, Minami-ku, Yokohama 232-8555, Japan; [7]Department of Pediatrics, Nagano Red Cross Hospital, 5-22-1 Wakasato, Nagano 380-8582, Japan; [8]Department of Pediatrics, Epilepsy Center, Nishi-Niigata Chuo National Hospital, Niigata 950-2085, Japan
[9]These authors contributed equally to this work
[10]Present address: Department of Neurology, Gunma Children's Medical Center, 779 Shimohakoda Hokkitsu-machi, Shibukawa, Gunma 377-8577, Japan
*Correspondence: naomat@yokohama-cu.ac.jp (N.M.), hsaitsu@yokohama-cu.ac.jp (H.S.)
http://dx.doi.org/10.1016/j.ajhg.2013.07.014.

Subjects and Methods

Subjects

Twelve individuals with OS were previously analyzed by whole-exome sequencing (WES).[3,11] In addition, we analyzed parental samples from 5 of the 12 individuals by WES. Screening for *GNAO1* mutations was performed in 367 individuals with epileptic encephalopathy (including 62 OS cases) by high-resolution-melting (HRM) analysis (339 cases) and/or WES (100 cases). The diagnosis was made on the basis of clinical features and characteristic patterns on EEG. Experimental protocols were approved by the institutional review board of Yokohama City University School of Medicine and Yamagata University Faculty of Medicine. Informed consent was obtained from the families of all individuals.

DNA Samples

Genomic DNA was obtained from peripheral-blood leukocytes by standard methods. For detection of a mosaic mutation in individual 2, genomic DNA from saliva and nails was isolated with an Oragene DNA kit (DNA Genotek) and an ISOHAIR kit (Nippon Gene), respectively.

WES

Genomic DNA was captured with the SureSelect Human All Exon v.4 Kit (Agilent Technologies) and sequenced with four samples per lane on an Illumina HiSeq 2000 (Illumina) with 101 bp paired-end reads. Image analysis and base calling were performed by Sequencing Control Software with Real-Time Analysis and CASAVA software v.1.8 (Illumina). Exome data processing, variant calling, and variant annotation were performed as previously described.[12–14] Reads were aligned to GRCh37 with Novoalign (Novocraft Technologies). Duplicate reads were removed with Picard, and local realignments around indels and base-quality-score recalibration were performed with the Genome Analysis Toolkit (GATK).[13] Single-nucleotide variants and small indels were identified with the GATK UnifiedGenotyper and were filtered according to the Broad Institute's best-practice guidelines v.3. Not flagged as clinically associated, variants registered in dbSNP135 were filtered. Filter-passed variants were annotated with ANNOVAR.[14] Pathogenic mutations detected by WES were confirmed by Sanger sequencing.

Mutation Screening

Genomic DNA was amplified with an illustra GenomiPhi V2 DNA Amplification Kit (GE Healthcare). Exons 1–8 covering the *GNAO1* coding region of two transcript variants (transcript variant 1, RefSeq accession number NM_020988.2, encoding $G\alpha_{o1}$; transcript variant 2, RefSeq accession number NM_138736.2, encoding $G\alpha_{o2}$) were screened by HRM analysis. The last two exons differ between the transcript variants. HRM analysis was performed with a Light Cycler 480 (Roche Diagnostics). Samples showing an aberrant melting curve in the HRM analysis were sequenced. PCR primers and conditions are shown in Table S1, available online. All mutations not present in publically available databases were verified with original genomic DNA and were searched for in the variant database of our 408 in-house control exomes.

Deep Sequencing of a Mosaic Mutation

PCR products (length 178 bp) spanning the c.521A>G mutation were amplified with the use of blood, saliva, and nail DNA samples from individual 2 and blood DNA samples from her parents as a template. Adaptor ligation, nick repair, and amplification were performed with the Ion Xpress Plus Fragment Library Kit (Life Technologies) according to the manufacturer's protocol (part no. 4471989 Rev. B). Indexing was carried out with the Xpress Barcode Adapters 1–16 Kit (Life Technologies). Emulsion PCR and enrichment steps were carried out with the Ion OneTouch 200 Template Kit v.2 (Life Technologies) according to the manufacturer's protocol (part no. 4478371 Rev. A). Sequencing of the amplicon libraries was carried out on the Ion Torrent Personal Genome Machine (PGM) with the Ion 314 sequencing chip and the Ion PGM 200 Sequencing Kit (Life Technologies) according to the recommended protocol (part no. 4474246 Rev. B). Torrent Suite 2.2 was used for all analyses. The percentage of mosaicism was examined with the Integrative Genomics Viewer.[15,16]

Expression Vectors

A full-length human *GNAO1* cDNA clone (transcript variant 1, encoding $G\alpha_{o1}$) was purchased from Kazusa DNA Research Institute. Human *GNAO1* cDNA was inserted into a pEF6/V5-His-C vector for the introduction of a C-terminal V5 epitope (Life Technologies). Site-directed mutagenesis using a KOD-Plus-Mutagenesis kit (Toyobo) was performed for generating *GNAO1* mutants, including c.521A>G (p.Asp174Gly), c.572_592del (p.The191_Phe197del), c.836T>A (p.Ile279Asn), and c.607G>A (p.Gly203Arg). A c.607_609delinsACA (p.Gly203Thr) mutant, in which GTP binding was reversible in contrast to the WT,[17] was also generated to serve as the known loss-of-function mutant.[18] All variant cDNAs were confirmed by Sanger sequencing.

Immunofluorescence Microscopy

Mouse neuroblastoma 2A (N2A) cells were grown as previously described.[4] N2A cells on glass coverslips were transfected with 200 ng of plasmid DNA with the use of X-tremeGENE 9 DNA Transfection Reagent (Roche Diagnostics). After 24 hr, cells were fixed in PBS containing 4% paraformaldehyde for 15 min and permeabilized in PBS containing 0.1% Triton X-100 for 5 min. Cells were then blocked with 10% normal goat serum for 30 min. V5-tagged $G\alpha_{o1}$ was detected with a mouse V5 antibody (1:200 dilution; Life Technologies) and Alexa-488-conjugated goat anti-mouse IgG (1:1000 dilution; Life Technologies). Coverslips were mounted with Vectashield (Vector Laboratories) that contained DAPI and were visualized with an inverted FV1000-D confocal microscope (Olympus).

Structural Modeling and Free-Energy Calculations

We used FoldX software (version 3.0β5) to construct mutated molecular structures and calculate the free-energy changes caused by the mutations.[19] We used crystal structures of the GDP-bound inactive $G\alpha_i\beta\gamma$ heterotrimer (Protein Data Bank [PDB] 1GG2),[20] the nucleotide-free $G\alpha_s\beta\gamma$ in complex with agonist-occupied monomeric β2 adrenergic receptor (β2AR) (PDB 3SN6),[21] and the transition-state analog of GTP ($GDP^+AlF_4^-$)-bound $G\alpha_q$ in complex with its effector phospholipase C-β (PLCβ) (PDB 3OHM)[22] as three-dimensional structure models of the $G\alpha_o$ subunit in different complexed states. Each of the mutations, corresponding to p.Asp174Gly, p.Ile279Asn, or p.Gly203Arg in the human $G\alpha_o$ subunit, was introduced into the Gα subunit of each complex, and the free-energy change upon the mutation was calculated with FoldX software. Note that ligands included in the complexes were ignored in the calculation because the FoldX energy function

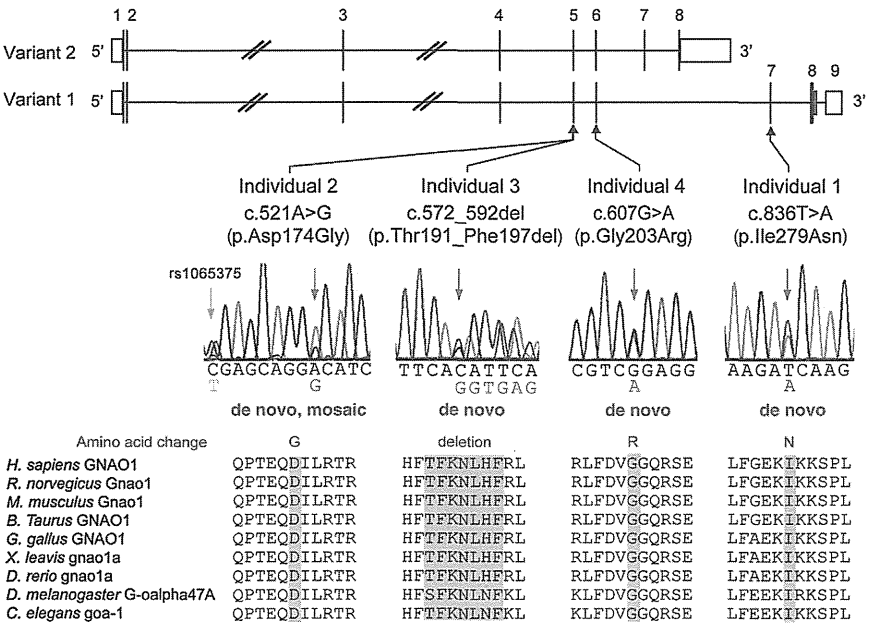

Figure 1. De Novo *GNAO1* Mutations in Individuals with Epileptic Encephalopathy
Schematic representation of *GNAO1*, including two transcript variants: transcript variant 1 (RefSeq NM_020988.2) with nine exons and transcript variant 2 (RefSeq NM_138736.2) with eight exons. The UTRs and coding regions are shown in white and black rectangles, respectively. Three mutations occurred in common exons of two transcript variants, and one mutation occurred uniquely in transcript variant 1. Note that the electropherogram of individual 2 suggested mosaicism of the c.521A>G mutation, and a heterozygous C>T change (rs1065375) was clearly demonstrated. All mutations caused substitution or deletion of evolutionarily conserved amino acids. Homologous sequences were aligned with the use of the CLUSTALW web site.

does not consider the contribution of ligands. The calculation was repeated three times, and the resultant data were presented as an average value with a SD.

Electrophysiology

For electrophysiological recording of calcium currents, we used NG108-15 cells transfected with individual *GNAO1* mutants. Expression vectors were introduced by electroporation with the Lonza Nucleofector device and the Cell Line Nucleofector Kit V (Lonza) according to the manufacture's protocol (program X-023). Two micrograms of plasmid DNA was used per transfection. The transfected cells were plated on poly-L-lysine-coated plastic coverslips (Cell Desk LF, MS-0113L; Sumitomo Bakelite) at a density of about 5×10^4 cells/cm^2 and cultured in Dulbecco's modified Eagle's medium (DMEM) supplemented with 10% fetal bovine serum (FBS). One day after transfection, the cells were differentiated with DMEM supplemented with 10 μM prostaglandin E1, 50 μM IBMX, and 1% FBS for 3–7 days before recording. During the culture period, half of the medium was changed every other day.

The recording was made by the perforated whole-cell patch-clamp technique with amphotericin B. Cells on coverslips were perfused under an Olympus BX51W upright microscope (Olympus) with a bath solution containing 140 mM NaCl, 5 mM $CaCl_2$, 4 mM KCl, 1 mM $MgCl_2$, 10 mM HEPES, 10 mM TEACl, 8 mM glucose, and 0.0002 mM tetrodotoxin (pH 7.3 adjusted with NaOH). The patch pipette solution contained 100 mM CsCl, 10 mM EGTA, and 40 mM HEPES (pH 7.3 adjusted with CsOH). Amphotericin B was added to the pipette solution at 2 μl/ml just before the experiments. The pipettes were fabricated from borosilicate glass capillaries and had a resistance of 4–8 MΩ when backfilled with the amphotericin-B-containing pipette solution. The recording was started when the series resistance was reduced to <150 MΩ after gigaseal formation and clear cellular capacitive surges had appeared. Voltage-gated calcium currents were elicited by the application of 50 ms depolarizing pulses to +10 mV from the holding potential of −65 mV, recorded with a Multiclamp 700B (Molecular Devices) controlled via pCLAMP10 software (Molecular Devices), filtered at 2 kHz, and sampled at 10 kHz with 50% compensation for series resistance. $G\alpha_o$-mediated current inhibition was elicited by the application of 10 μM norepinephrine via the bath solution. After 3–5 min, inhibition was assessed by measurement of the changes in current density just before the end of the depolarizing pulses. Recordings were made at room temperature.

Statistical multiple comparisons were made with ANOVA followed by Dunnett's post hoc test, and the threshold p value for judging statistical significance was 0.05. The current inhibition induced by norepinephrine in individual mutant-expressing cells was assessed with a paired t test. The results are given as the mean ± SEM.

Results

GNAO1 Is Mutated in Individuals with Epileptic Encephalopathy

We previously performed WES of 12 individuals with OS.[3,11] In this study, we analyzed parental samples from 5 of the 12 individuals by WES (mean RefSeq read depth of 109) to systematically screen de novo or recessive mutations. We found no recessive mutations in *SLC25A22* (MIM 609302), *PNPO* (MIM 610090), *PNKP* (MIM 613402), *PLCB1* (MIM 613722), or *ST3GAL3* (MIM 615006), whose mutations were previously found in epileptic encephalopathy,[23–27] but we did find one or two de novo mutations in each of the five trio exomes. Among them, a de novo missense mutation (c.836T>A [p.Ile279Asn]) in *GNAO1* at 16q12.2 was identified in individual 1. In the exome data of the other seven original individuals, we also found in individual 2 a second missense mutation (c.521A>G [p.Asp174Gly]), which was confirmed as a de novo event by Sanger sequencing (Figure 1). Moreover, *GNAO1* mutation screening in 367 individuals with epileptic encephalopathy by HRM analysis (339 individuals) and/or WES (100 individuals,

Table 1. Clinical Features of Individuals with a *GNAO1* Mutation

	Individual 1	Individual 2	Individual 3	Individual 4
Gender	female	female	female	female
Age	13 years	4 years, 1 month	died at 11 months	8 years
Mutation	c.836T>A (p.Ile279Asn)	c.521A>G (p.Asp174Gly)	c.572_592 del (p.Thr191_Phe197 del)	c.607G>A (p.Gly203Arg)
Inheritance	de novo	de novo, somatic mosaic	de novo	de novo
Diagnosis	Ohtahara syndrome	Ohtahara syndrome	Ohtahara syndrome	epileptic encephalopathy
Initial symptom	tonic seizure at 4 days	series of tonic seizures at 29 days (tonic upgaze, head nodding, extension of all extremities)	series of tonic seizures at 2 weeks (resemble spasms)	opisthotonic posture, developmental delay at 7 months
Initial EEG	suppression-burst pattern at 4 days	suppression-burst pattern at 29 days	suppression-burst pattern at 2 weeks	diffuse irregular spike-and-slow-wave complex at 5 years
Course of seizures	tonic seizure at 5 years	series of tonic seizures at 9 months	tonic seizure at 10 months	focal seizure (tonic upgaze), tonic seizure at 5 years
Course of EEG	multifocal sharp waves at 1 year, 4 months; suppression-burst pattern at 5 years, 6 months	hypsarrhythmia at 3 months; diffuse spike-and-slow-wave complex at 1 year, 7 months; sharp waves at frontal lobe at 3 years, 9 months	hypsarrhythmia at 4 months	not done
Involuntary movement	-	-	dystonia	severe chorea, athetosis
Seizure control	intractable (2–3 times per day)	intractable (0–2 times per day)	intractable	intractable (several times per day)
Development				
Head control	-	+	-	-
Sitting	-	-	-	-
Meaningful words	-	-	-	-
MRI	normal at 1 month; cerebral atrophy at 5 years, 6 months	delayed myelination and thin corpus callosum at 10 months	normal at 3 months	delayed myelination at 1 year, 3 months; reduced cerebral white matter, thin corpus callosum at 4 years, 8 months

mean read depth of 129) revealed two de novo mutations: c.572_592 del (p.Thr191_Phe197del) in individual 3 and c.607G>A (p.Gly203Arg) in individual 4 (Figure 1). One mutation (c.836T>A) specifically affects *GNAO1* transcript variant 1, whereas the other three mutations affect both transcript variants 1 and 2. Web-based prediction tools suggested that these four mutations would be pathogenic (Table S2). None of the four mutations was found in the 6,500 exomes of the National Heart, Lung, and Blood Institute (NHLBI) Exome Sequencing Project Exome Variant Server or among our 408 in-house control exomes. Interestingly, exome data and Sanger sequencing indicated that the c.521A>G mutation in individual 2 was somatic mosaic (Figure 1 and Table S3). We confirmed de novo somatic mosaicism of the c.521A>G mutation by deep sequencing of PCR products amplified with blood, nail, and saliva DNA from individual 2 and blood DNA from her parents, showing that approximately 35%–50% of cells harbored the mutation (Table S3).

Phenotypes Associated with *GNAO1* Mutations

Neurological features of four female individuals with *GNAO1* mutations are shown in Table 1. Three individuals (individuals 1–3) developed tonic seizures with suppression-burst pattern on EEG at the onset (range 4–29 days), leading to a diagnosis of OS. Individuals 2 and 3 transited to West syndrome, a common infantile epileptic syndrome, as revealed by hypsarrhythmia on EEG at 3–4 months of age (Figures 2A–2C). Individual 4 showed developmental delay and opisthotonic posture at 7 months of age, and complex partial seizures with epileptic discharge on EEG was observed at 5 years (Figure 2D). Of note, two individuals showed involuntary movements: individual 3 showed dystonia, and individual 4 displayed chorea and athetosis (Table 1 and Movie S1). Brain MRI showed delayed myelination in individuals 2 and 4, cerebral atrophy or reduced cerebral white matter in individuals 1 and 4, and thin corpus callosum in individuals 2 and 4 (Figures 2E–2I). Although seizures and EEG

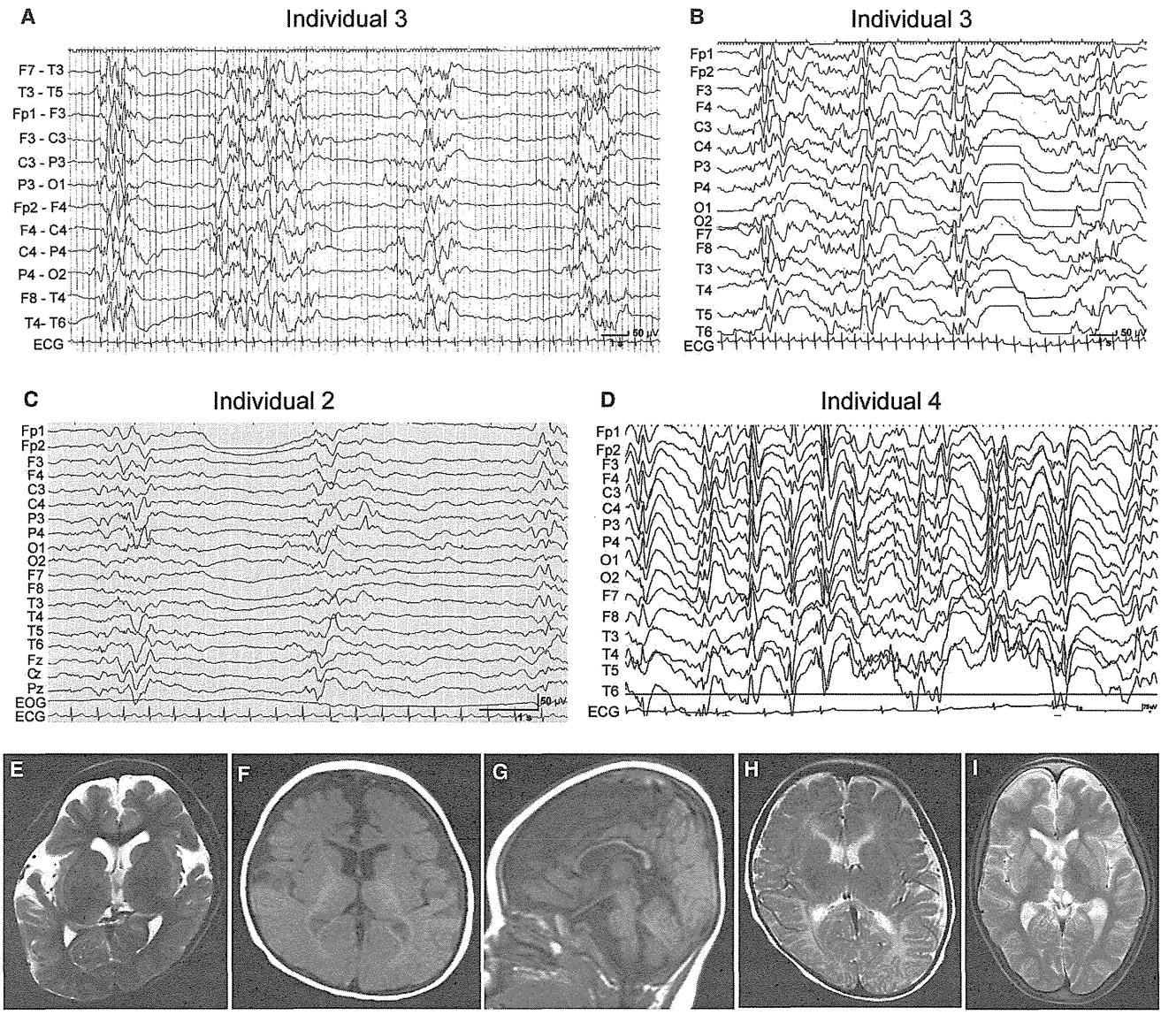

Figure 2. EEG and Brain MRI Features of Individuals with *GNAO1* Mutations
(A and B) Interictal EEG of individual 3. A suppression-burst pattern was observed at 2 months of age (A), and transition to hypsarrhythmia was observed at 4 months (B).
(C) Interictal EEG of individual 2 shows a suppression-burst pattern at 2 months.
(D) Interictal EEG of individual 4 shows a diffuse spike- or sharp-and-slow-wave complex at 5 years.
(E–I) T2-weighted axial images through the basal ganglia (E, H, and I) and T1-weighted axial (F) and sagittal (G) images. Individual 1 showed cerebral atrophy at 5 years and 6 months (E). Individual 2 showed delayed myelination and thin corpus callosum at 10 months (F and G). Individual 3 showed normal appearance at 3 months (H). Individual 4 showed reduced white matter at 7 years (I).

findings in two individuals with OS (individuals 2 and 3) were temporarily improved by adrenocorticotropic hormone therapy and valproic acid, all four individuals had intractable epileptic seizures in spite of combinatory therapy of antiepileptic drugs. All individuals had severe intellectual disability and motor developmental delay, and individual 3 died at 11 months because of respiratory-tract obstruction. These data suggest that *GNAO1* mutations can cause multiple neurodevelopmental phenotypes, including epileptic encephalopathy and involuntary movements.

Expression of Mutant $G\alpha_{o1}$ in N2A Cells

To examine the mutational effect of four *GNAO1* mutations, we performed transient expression experiments in N2A cells (Figure 3). C-terminally V5-epitope-tagged wild-type (WT) $G\alpha_{o1}$, encoded by transcript variant 1, was clearly localized in the cell periphery, as previously reported.[28] The p.Gly203Thr (with known loss of function)[17] and p.Gly203Arg (in individual 4) altered proteins were also localized in the cell periphery. In contrast, the p.Thr191_Phe197del altered protein (in individual 3) accumulated in the cytosolic compartment. The p.Asp174Gly

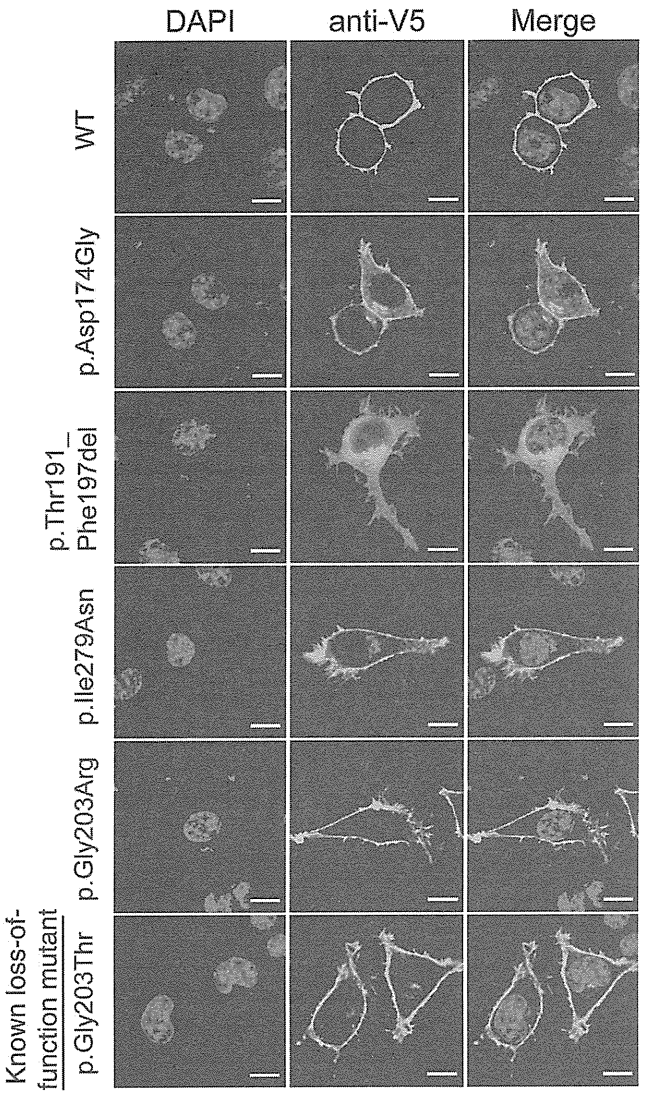

Figure 3. Localization of V5-Tagged $G\alpha_{o1}$ Proteins in N2A Cells
Localization of WT and five altered $G\alpha_{o1}$ proteins in N2A cells. The WT and p.Gly203Arg and p.Gly203Thr altered proteins were localized to the cell periphery. In contrast, the p.Thr191_Phe197del protein was localized to the cytosolic compartment. The other p.Asp174Gly and p.Ile279Asn proteins were localized to the cell periphery but were also observed in the cytosol. The scale bars represent 10 μm.

(individual 2) and p.Ile279Asn (individual 1) altered proteins were localized to the cell periphery and had weak signal in the cytosol, where more intense signal was observed in the p.Asp174Gly protein. Similar patterns of localization were observed for C-terminally AcGFP1-tagged $G\alpha_{o1}$ (Figure S1). These localization patterns suggest that the function of the p.Thr191_Phe197del altered protein might be most severely affected.

Structural Impacts of the Mutations on the Gα-Containing Complexes

To evaluate the impact of the *GNAO1* mutations on specific functions at the atomic level, we mapped the substituted positions onto structures of the Gα subunit in complexed states representing the GDP-bound inactive state, the nucleotide-free $G\alpha_s\beta\gamma$ in complex with the receptor, and the GTP-bound active state. In the case of point mutations, we further estimated free-energy changes of the mutations by using FoldX software (version 3.0β5).[19]

The region corresponding to amino acid residues 191–197 of human $G\alpha_{o1}$ is located in β strands and their connecting loop region and is involved in interactions with the G-protein-coupled receptor (GPCR) in the $G\alpha\beta\gamma$-β2AR complex (Figure 4A and Figure S2A). Thus, the deletion would affect secondary structure of the molecule and would not only impair the interaction with GPCR but also severely destabilize the Gα-subunit fold. The substituted residues corresponding to Asp174 and Ile279 of the human $G\alpha_{o1}$ subunit are both buried inside the protein (Figure 4A) and are involved in hydrogen-bonding and hydrophobic interactions, respectively (Figure S2B). Therefore, the p.Asp174Gly and p.Ile279Asn substitutions would destabilize the Gα-subunit fold, as supported by FoldX calculations showing a more than 2 kcal/mol increase in free-energy changes for these substitutions (Figure 4B). It can be speculated that these altered proteins tend to be misfolded or denatured in N2A cells and thus have altered cellular localization (Figure 3).

The substituted residue corresponding to Gly203 of human $G\alpha_{o1}$ is located within the highly conserved switch II region, responsible for activation of downstream effectors upon GTP binding (Figure 4A). Conformations of the switch regions differ depending on the complex state of the G protein. In the $G\alpha\beta\gamma$ heterotrimer and the $GDP^{+}AlF_4^{-}$-bound Gα-effector (PLCβ) complex, the glycine residues are closely surrounded by the switch I region and GTP (Figure 4A and Figure S2C). Thus, the p.Gly203Arg substitution would cause steric hindrance between the arginine side chain and the switch I region and/or GTP, destabilizing the complex, as supported by the FoldX calculations showing a remarkable increase in free-energy change upon the p.Gly203Arg substitution. By contrast, in the $G\alpha\beta\gamma$-receptor (β2AR) complex, no substantial steric hindrance was predicted from the structural modeling and FoldX calculations (Figure 4B and Figure S2C). These findings suggest that the p.Gly203Arg-substituted Gα subunit would impair GTP binding and/or activation of the downstream effectors, although it might still bind to GPCR. This prediction was supported by previous reports, in which GTP binding was weakened in the p.Gly203Thr altered Gα.[17] This also appears to be consistent with the apparently normal cellular localization of the p.Gly203Arg altered protein in N2A cells (Figure 3).

Electrophysiological Evaluation of $G\alpha_{o1}$ Mutants

It has been reported that N-type calcium channels are inhibited, at least in part, via $G\alpha_o$-mediated signaling.[7] Using NG108-15 cells, in which norepinephrine-induced calcium-current inhibition is mediated by $G\alpha_o$ (Figure 5A),[29] we analyzed functional properties of altered $G\alpha_{o1}$. Compared with cells expressing WT $G\alpha_{o1}$ (the

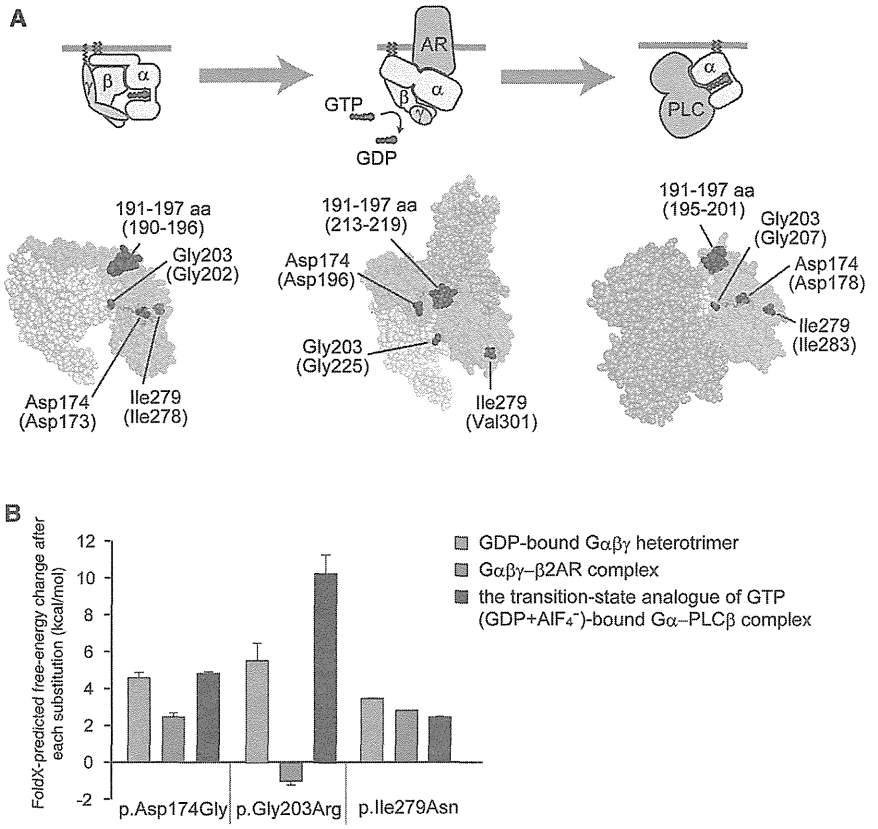

Figure 4. Structural Consideration of the Gα Amino Acid Substitutions in Some Complexed States

(A) Map of the amino acid substitution sites on the crystal structures of Gα-containing complexes: the GDP-bound inactive $G\alpha_i\beta\gamma$ heterotrimer (left), the nucleotide-free $G\alpha_s\beta\gamma$ in complex with an agonist-occupied monomeric β2AR (center), and the $GDP^{+}AlF_4^{-}$-bound $G\alpha_q$ in complex with its effector PLCβ (right). Molecular structures are shown as space-filling representations (from PyMOL). Gα, Gβ, and Gγ subunits are colored green, yellow, and pink, respectively, and the switch I and switch II regions in the Gα subunit are in light green. The β2AR (center) and PLCβ (right) molecules are colored brown. The substituted sites are shown in red, and the indicated amino acid numbers correspond to human $G\alpha o_1$ and, in parentheses, rat $G\alpha i_1$ (UniProtKB/Swiss-Prot P10824) (left), bovine Gαs (UniProtKB/Swiss-Prot P04896) (center), and mouse Gαq (UniProtKB/Swiss-Prot P21279) (right). The illustrations above each model show the orientation of each subunit and the bound molecules.

(B) The free-energy change after each of the amino acid substitutions was estimated from calculations using FoldX software. Each error bar represents an average value with a SD.

leftmost column in Figure 5B), NG108-15 cells expressing the p.Thr191_Phe197del substitution revealed a significant increase in calcium-current density before application of norepinephrine ($p < 0.05$ by Dunnett's post hoc test; the second column from the right in Figure 5B), suggesting that localization of the altered $G\alpha_{o1}$ might affect calcium-channel activity. In cells expressing the p.Asp174Gly substitution, a mild increase in the current density was also suggested, although the difference was not significant (the third column from the left in Figure 5B). The other two substitutions had no effects on the current (the second column from the left and the rightmost column in Figure 5B). Treatment with 10 μM norepinephrine reduced the calcium-current density by 19.0% ± 5.0% in cells expressing WT $G\alpha_{o1}$ ($p < 0.01$ by paired t test; left panel in Figure 5A and the leftmost bar in Figure 5C). A similar reduction was observed in cells expressing the p.Ile279Asn alteration (18.5% ± 3.5%, $p < 0.01$ by paired t test; the rightmost bar in Figure 5C). In cells expressing the p.Thr191_Phe197del alteration, by contrast, the reduction was obscured (12.1% ± 5.0%, not significant by paired t test; right panel in Figure 5A and the second bar from the right in Figure 5C). In cells expressing the other two substitutions (p.Gly203Thr and p.Asp174Gly), weaker current inhibition by norepinephrine was suggested (9.9% ± 3.8% and 11.1% ± 3.5%, respectively; both were $p < 0.05$ by paired t test; the second and third bars from the left in Figure 5C), although compared with that in WT-expressing cells, the degrees of inhibition in Gly203Thr- and p.Asp174Gly-expressing cells did not reach statistical significance (not significant by ANOVA). These data suggest that *GNAO1* mutations could hamper $G\alpha_o$-mediated signaling.

Discussion

We successfully identified four de novo heterozygous missense *GNAO1* mutations in four individuals. All four individuals showed severe intellectual disability and motor developmental delay, demonstrating that aberration of $G\alpha_o$ affects intellectual and motor development. In addition, all four individuals showed epileptic encephalopathy, and two of them showed involuntary movements. Because $G\alpha_o$-deficient mice show occasional seizures and generalized tremor,[9,10] it is likely that epilepsy and involuntary movement are two of the characteristic features caused by *GNAO1* mutations. Although $G\alpha_o$-deficient mice also show hyperactivity and hyperalgesia,[10] it is difficult to evaluate whether our individuals had these symptoms because of severe motor and cognitive impairment.

All four of these mutations, and especially two mutations leading to the p.Thr191_Phe197del and p.Gly203Arg substitutions, are predicted to affect $G\alpha_o$ function by structural evaluation. In fact, transient expression in N2A cells showed that localization of the p.Thr191_Phe197del altered protein was dramatically changed to the cytosolic compartment. Interestingly, two alterations (p.Ile279Asn

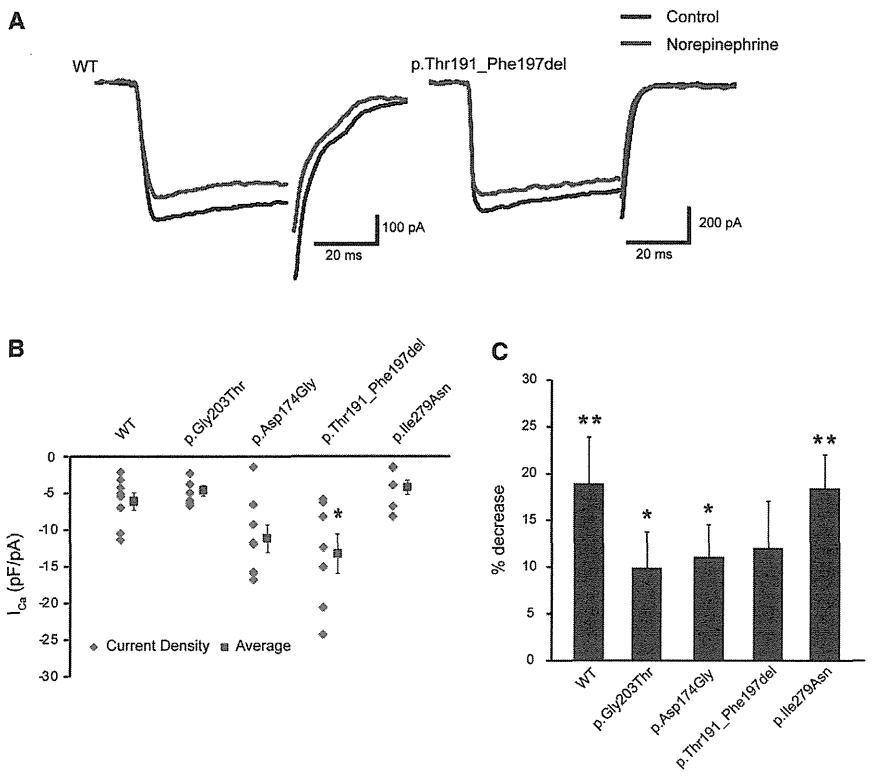

Figure 5. Evaluation of $G\alpha_o$-Mediated Signaling in NG108-15 Cell Calcium-Current Generation

(A) Representative traces of voltage-gated calcium currents generated in NG108-15 cells expressing WT (left) or p.Thr191_Phe197del altered (right) $G\alpha_{o1}$. Black and red traces represent the currents before and 3 min after application of 10 μM norepinephrine, respectively.

(B) Current densities of the calcium currents before norepinephrine treatment in cells expressing WT or altered $G\alpha_{o1}$. Scatter plots represent the densities in individual cells. Red squares and bars represent the means and SEMs, respectively, of the densities in individual cell groups (WT, n = 8; p.Gly203Thr, n = 7; p.Asp174Gly, n = 8; p.Thr191_Phe197del, n = 7; p.Ile279Asn, n = 7). Compared with that in cells expressing WT $G\alpha_{o1}$, the current density in cells expressing p.Thr191_Phe197del increased significantly (*$p < 0.05$ by Dunnett's post hoc test). The densities in the cells expressing other altered proteins did not vary significantly.

(C) Comparison of norepinephrine-induced inhibition of calcium currents in cells expressing altered $G\alpha_{o1}$. Each error bar represents the mean and SEM of the percent decrease in current density induced by application of 10 μM norepinephrine. Paired t tests indicated that the inhibition induced by norepinephrine was significant in cells expressing WT (n = 8) and p.Gly203Thr (n = 7), p.Asp174Gly (n = 8), and p.Ile279Asn (n = 7) altered proteins (**$p < 0.01$ and *$p < 0.05$), but not in cells expressing p.Thr191_Phe197del (n = 7). Although there was some tendency for decreased inhibition in cells expressing altered proteins, the tendency did not reach statistical significance compared with that in WT-expressing cells ($p = 0.41$ by ANOVA).

and p.Asp174Gly) also showed weak signal in the cytosol, suggesting that localization to the plasma membrane was variably impaired in three altered proteins. Measurement of voltage-dependent calcium currents in NG108-15 cells also suggested impaired functions of altered $G\alpha_{o1}$. The p.Thr191_Phe197del alteration significantly increased the basal calcium-current density, and compared with WT-expressing cells, cells expressing one of the three substitutions (p.Thr191_Phe197del, p.Asp174Gly, or p.Gly203Thr) showed a tendency towards weaker inhibition of calcium currents by norepinephrine. All these data suggest that the four *GNAO1* mutations might cause loss of $G\alpha_{o1}$ function.

Our experimental data suggest that $G\alpha_o$ function might be most severely affected in the p.Thr191_Phe197del altered protein. This appears to be correlated with the severity of clinical features because individual 3 showed both OS and involuntary movements and indeed died during the infantile period. Therefore, she might have had the most severe phenotype caused by a *GNAO1* mutation. Another interesting finding is somatic mosaicism of the c.521A>G (p.Asp174Gly) mutation in individual 2, in whom approximately 35%–50% of cells harbored the mutation. Somatic mosaicism of responsive genes in infantile epilepsy, such as *SCN1A* (MIM 182389) and *STXBP1*, have been reported, explaining the presence of unaffected or mildly affected transmitting parents.[30,31] However, individual 2 showed OS, delayed myelination, and thin corpus callosum. Although we did not determine the mosaic rate in brain tissues, the presence of 35%–50% of cells harboring the *GNAO1* mutation in the brain might be sufficient to cause abnormal brain development.

It has been reported that activation of G-protein-coupled α_2 adrenergic receptors by norepinephrine attenuates epileptiform activity in the hippocampal CA3 region.[32] $G\alpha_o$ is known to be involved in this response,[33] suggesting that alteration of pathways mediated by α_2 adrenergic receptor and $G\alpha_o$ might contribute to the pathogenesis of epilepsy. Because calcium-current inhibition is a well-known consequence of $G\alpha_o$-mediated signaling induced by norepinephrine, it is possible that epileptic seizures associated with *GNAO1* mutations might be improved by calcium-channel modulators. For example, pregabalin and gabapentin act as selective calcium-channel blockers,[34,35] and topiramate modulates high-voltage-activated calcium channels in dentate granule cells.[36] Because our four individuals were not treated with these drugs, it is worth administrating these three drugs for examining putative protective effects.

In conclusion, de novo heterozygous *GNAO1* mutations were identified in four individuals with epileptic encephalopathy. Furthering our understanding of abnormal

$G\alpha_o$-mediated heterotrimeric G protein signaling might provide new insights into the pathogenesis and treatment of epileptic encephalopathy.

Supplemental Data

Supplemental Data include two figures, three tables, and one movie and can be found with this article online at http://www.cell.com/AJHG.

Acknowledgments

We would like to thank the individuals and their families for their participation in this study. We also thank Aya Narita and Nobuko Watanabe for their technical assistance and Tohru Kozasa and Nobuchika Suzuki for their valuable comments. This work was supported by the Ministry of Health, Labour, and Welfare of Japan, the Japan Society for the Promotion of Science (Grants-in-Aid for Scientific Research (B) [25293085 and 25293235] and a Grant-in-Aid for Scientific Research (A) [13313587]), the Takeda Science Foundation, the Japan Science and Technology Agency, the Strategic Research Program for Brain Sciences (11105137), and a Grant-in-Aid for Scientific Research on Innovative Areas (Transcription Cycle) from the Ministry of Education, Culture, Sports, Science, and Technology of Japan (12024421).

Received: May 17, 2013
Revised: July 9, 2013
Accepted: July 17, 2013
Published: August 29, 2013

Web Resources

The URLs for data presented herein are as follows:

CLUSTALW, http://www.genome.jp/tools/clustalw/
GenBank, http://www.ncbi.nlm.nih.gov/Genbank/
NHLBI Exome Sequencing Project (ESP) Exome Variant Server, http://evs.gs.washington.edu/EVS/
Online Mendelian Inheritance in Man (OMIM), http://www.omim.org/
Picard, http://picard.sourceforge.net/
Protein Data Bank, http://www.rcsb.org/pdb/home/home.do
PyMOL, www.pymol.org
RefSeq, http://www.ncbi.nlm.nih.gov/RefSeq
UniProtKB/Swiss-Prot, http://www.uniprot.org/

References

1. Dulac, O. (2001). Epileptic encephalopathy. Epilepsia *42* (*Suppl 3*), 23–26.
2. Ohtahara, S., and Yamatogi, Y. (2006). Ohtahara syndrome: with special reference to its developmental aspects for differentiating from early myoclonic encephalopathy. Epilepsy Res. *70* (*Suppl 1*), S58–S67.
3. Saitsu, H., Kato, M., Koide, A., Goto, T., Fujita, T., Nishiyama, K., Tsurusaki, Y., Doi, H., Miyake, N., Hayasaka, K., and Matsumoto, N. (2012). Whole exome sequencing identifies *KCNQ2* mutations in Ohtahara syndrome. Ann. Neurol. *72*, 298–300.
4. Saitsu, H., Kato, M., Mizuguchi, T., Hamada, K., Osaka, H., Tohyama, J., Uruno, K., Kumada, S., Nishiyama, K., Nishimura, A., et al. (2008). *De novo* mutations in the gene encoding STXBP1 (MUNC18-1) cause early infantile epileptic encephalopathy. Nat. Genet. *40*, 782–788.
5. Weckhuysen, S., Mandelstam, S., Suls, A., Audenaert, D., Deconinck, T., Claes, L.R., Deprez, L., Smets, K., Hristova, D., Yordanova, I., et al. (2012). *KCNQ2* encephalopathy: emerging phenotype of a neonatal epileptic encephalopathy. Ann. Neurol. *71*, 15–25.
6. Kato, M., Saitoh, S., Kamei, A., Shiraishi, H., Ueda, Y., Akasaka, M., Tohyama, J., Akasaka, N., and Hayasaka, K. (2007). A longer polyalanine expansion mutation in the *ARX* gene causes early infantile epileptic encephalopathy with suppression-burst pattern (Ohtahara syndrome). Am. J. Hum. Genet. *81*, 361–366.
7. Wettschureck, N., and Offermanns, S. (2005). Mammalian G proteins and their cell type specific functions. Physiol. Rev. *85*, 1159–1204.
8. Huff, R.M., Axton, J.M., and Neer, E.J. (1985). Physical and immunological characterization of a guanine nucleotide-binding protein purified from bovine cerebral cortex. J. Biol. Chem. *260*, 10864–10871.
9. Valenzuela, D., Han, X., Mende, U., Fankhauser, C., Mashimo, H., Huang, P., Pfeffer, J., Neer, E.J., and Fishman, M.C. (1997). G alpha(o) is necessary for muscarinic regulation of Ca2+ channels in mouse heart. Proc. Natl. Acad. Sci. USA *94*, 1727–1732.
10. Jiang, M., Gold, M.S., Boulay, G., Spicher, K., Peyton, M., Brabet, P., Srinivasan, Y., Rudolph, U., Ellison, G., and Birnbaumer, L. (1998). Multiple neurological abnormalities in mice deficient in the G protein Go. Proc. Natl. Acad. Sci. USA *95*, 3269–3274.
11. Saitsu, H., Kato, M., Osaka, H., Moriyama, N., Horita, H., Nishiyama, K., Yoneda, Y., Kondo, Y., Tsurusaki, Y., Doi, H., et al. (2012). *CASK* aberrations in male patients with Ohtahara syndrome and cerebellar hypoplasia. Epilepsia *53*, 1441–1449.
12. Saitsu, H., Nishimura, T., Muramatsu, K., Kodera, H., Kumada, S., Sugai, K., Kasai-Yoshida, E., Sawaura, N., Nishida, H., Hoshino, A., et al. (2013). *De novo* mutations in the autophagy gene *WDR45* cause static encephalopathy of childhood with neurodegeneration in adulthood. Nat. Genet. *45*, 445–449, e1.
13. DePristo, M.A., Banks, E., Poplin, R., Garimella, K.V., Maguire, J.R., Hartl, C., Philippakis, A.A., del Angel, G., Rivas, M.A., Hanna, M., et al. (2011). A framework for variation discovery and genotyping using next-generation DNA sequencing data. Nat. Genet. *43*, 491–498.
14. Wang, K., Li, M., and Hakonarson, H. (2010). ANNOVAR: functional annotation of genetic variants from high-throughput sequencing data. Nucleic Acids Res. *38*, e164.
15. Robinson, J.T., Thorvaldsdóttir, H., Winckler, W., Guttman, M., Lander, E.S., Getz, G., and Mesirov, J.P. (2011). Integrative genomics viewer. Nat. Biotechnol. *29*, 24–26.
16. Thorvaldsdóttir, H., Robinson, J.T., and Mesirov, J.P. (2013). Integrative Genomics Viewer (IGV): high-performance genomics data visualization and exploration. Brief. Bioinform. *14*, 178–192.
17. Slepak, V.Z., Wilkie, T.M., and Simon, M.I. (1993). Mutational analysis of G protein alpha subunit G(o) alpha expressed in Escherichia coli. J. Biol. Chem. *268*, 1414–1423.
18. Williams, D.J., Puhl, H.L., and Ikeda, S.R. (2010). A Simple, Highly Efficient Method for Heterologous Expression in Mammalian Primary Neurons Using Cationic Lipid-mediated mRNA Transfection. Front Neurosci. *4*, 181.

19. Guerois, R., Nielsen, J.E., and Serrano, L. (2002). Predicting changes in the stability of proteins and protein complexes: a study of more than 1000 mutations. J. Mol. Biol. *320*, 369–387.
20. Wall, M.A., Coleman, D.E., Lee, E., Iñiguez-Lluhi, J.A., Posner, B.A., Gilman, A.G., and Sprang, S.R. (1995). The structure of the G protein heterotrimer Gi alpha 1 beta 1 gamma 2. Cell *83*, 1047–1058.
21. Rasmussen, S.G., DeVree, B.T., Zou, Y., Kruse, A.C., Chung, K.Y., Kobilka, T.S., Thian, F.S., Chae, P.S., Pardon, E., Calinski, D., et al. (2011). Crystal structure of the β2 adrenergic receptor-Gs protein complex. Nature *477*, 549–555.
22. Waldo, G.L., Ricks, T.K., Hicks, S.N., Cheever, M.L., Kawano, T., Tsuboi, K., Wang, X., Montell, C., Kozasa, T., Sondek, J., and Harden, T.K. (2010). Kinetic scaffolding mediated by a phospholipase C-beta and Gq signaling complex. Science *330*, 974–980.
23. Edvardson, S., Baumann, A.M., Mühlenhoff, M., Stephan, O., Kuss, A.W., Shaag, A., He, L., Zenvirt, S., Tanzi, R., Gerardy-Schahn, R., and Elpeleg, O. (2013). West syndrome caused by ST3Gal-III deficiency. Epilepsia *54*, e24–e27.
24. Molinari, F., Raas-Rothschild, A., Rio, M., Fiermonte, G., Encha-Razavi, F., Palmieri, L., Palmieri, F., Ben-Neriah, Z., Kadhom, N., Vekemans, M., et al. (2005). Impaired mitochondrial glutamate transport in autosomal recessive neonatal myoclonic epilepsy. Am. J. Hum. Genet. *76*, 334–339.
25. Mills, P.B., Surtees, R.A., Champion, M.P., Beesley, C.E., Dalton, N., Scambler, P.J., Heales, S.J., Briddon, A., Scheimberg, I., Hoffmann, G.F., et al. (2005). Neonatal epileptic encephalopathy caused by mutations in the PNPO gene encoding pyridox(am)ine 5′-phosphate oxidase. Hum. Mol. Genet. *14*, 1077–1086.
26. Shen, J., Gilmore, E.C., Marshall, C.A., Haddadin, M., Reynolds, J.J., Eyaid, W., Bodell, A., Barry, B., Gleason, D., Allen, K., et al. (2010). Mutations in PNKP cause microcephaly, seizures and defects in DNA repair. Nat. Genet. *42*, 245–249.
27. Kurian, M.A., Meyer, E., Vassallo, G., Morgan, N.V., Prakash, N., Pasha, S., Hai, N.A., Shuib, S., Rahman, F., Wassmer, E., et al. (2010). Phospholipase C beta 1 deficiency is associated with early-onset epileptic encephalopathy. Brain *133*, 2964–2970.
28. Nakata, H., and Kozasa, T. (2005). Functional characterization of Galphao signaling through G protein-regulated inducer of neurite outgrowth 1. Mol. Pharmacol. *67*, 695–702.
29. McFadzean, I., Mullaney, I., Brown, D.A., and Milligan, G. (1989). Antibodies to the GTP binding protein, Go, antagonize noradrenaline-induced calcium current inhibition in NG108-15 hybrid cells. Neuron *3*, 177–182.
30. Saitsu, H., Hoshino, H., Kato, M., Nishiyama, K., Okada, I., Yoneda, Y., Tsurusaki, Y., Doi, H., Miyake, N., Kubota, M., et al. (2011). Paternal mosaicism of an *STXBP1* mutation in OS. Clin. Genet. *80*, 484–488.
31. Marini, C., Scheffer, I.E., Nabbout, R., Suls, A., De Jonghe, P., Zara, F., and Guerrini, R. (2011). The genetics of Dravet syndrome. Epilepsia *52* (*Suppl 2*), 24–29.
32. Jurgens, C.W., Hammad, H.M., Lichter, J.A., Boese, S.J., Nelson, B.W., Goldenstein, B.L., Davis, K.L., Xu, K., Hillman, K.L., Porter, J.E., and Doze, V.A. (2007). Alpha2A adrenergic receptor activation inhibits epileptiform activity in the rat hippocampal CA3 region. Mol. Pharmacol. *71*, 1572–1581.
33. Goldenstein, B.L., Nelson, B.W., Xu, K., Luger, E.J., Pribula, J.A., Wald, J.M., O'Shea, L.A., Weinshenker, D., Charbeneau, R.A., Huang, X., et al. (2009). Regulator of G protein signaling protein suppression of Galphao protein-mediated alpha2A adrenergic receptor inhibition of mouse hippocampal CA3 epileptiform activity. Mol. Pharmacol. *75*, 1222–1230.
34. Sills, G.J. (2006). The mechanisms of action of gabapentin and pregabalin. Curr. Opin. Pharmacol. *6*, 108–113.
35. Stefani, A., Spadoni, F., Giacomini, P., Lavaroni, F., and Bernardi, G. (2001). The effects of gabapentin on different ligand- and voltage-gated currents in isolated cortical neurons. Epilepsy Res. *43*, 239–248.
36. Zhang, X., Velumian, A.A., Jones, O.T., and Carlen, P.L. (2000). Modulation of high-voltage-activated calcium channels in dentate granule cells by topiramate. Epilepsia *41* (*Suppl 1*), S52–S60.

ARTICLE

Mutations in *KLHL40* Are a Frequent Cause of Severe Autosomal-Recessive Nemaline Myopathy

Gianina Ravenscroft,[1,28] Satoko Miyatake,[2,28] Vilma-Lotta Lehtokari,[3,4] Emily J. Todd,[1] Pauliina Vornanen,[3,4] Kyle S. Yau,[1] Yukiko K. Hayashi,[5] Noriko Miyake,[2] Yoshinori Tsurusaki,[2] Hiroshi Doi,[2] Hirotomo Saitsu,[2] Hitoshi Osaka,[6] Sumimasa Yamashita,[6] Takashi Ohya,[7] Yuko Sakamoto,[7] Eriko Koshimizu,[2] Shintaro Imamura,[8] Michiaki Yamashita,[8] Kazuhiro Ogata,[9] Masaaki Shiina,[9] Robert J. Bryson-Richardson,[10] Raquel Vaz,[10] Ozge Ceyhan,[11] Catherine A. Brownstein,[11] Lindsay C. Swanson,[11] Sophie Monnot,[12] Norma B. Romero,[13] Helge Amthor,[12] Nina Kresoje,[14] Padma Sivadorai,[15] Cathy Kiraly-Borri,[16] Goknur Haliloglu,[17] Beril Talim,[17] Diclehan Orhan,[18] Gulsev Kale,[18] Adrian K. Charles,[19] Victoria A. Fabian,[15] Mark R. Davis,[15] Martin Lammens,[20] Caroline A. Sewry,[21] Adnan Manzur,[21] Francesco Muntoni,[21] Nigel F. Clarke,[22] Kathryn N. North,[23] Enrico Bertini,[24] Yoram Nevo,[25] Ekkhard Willichowski,[26] Inger E. Silberg,[27] Haluk Topaloglu,[17] Alan H. Beggs,[11] Richard J.N. Allcock,[14] Ichizo Nishino,[5] Carina Wallgren-Pettersson,[3,4] Naomichi Matsumoto,[2,29,*] and Nigel G. Laing[1,29,*]

Nemaline myopathy (NEM) is a common congenital myopathy. At the very severe end of the NEM clinical spectrum are genetically unresolved cases of autosomal-recessive fetal akinesia sequence. We studied a multinational cohort of 143 severe-NEM-affected families lacking genetic diagnosis. We performed whole-exome sequencing of six families and targeted gene sequencing of additional families. We identified 19 mutations in *KLHL40* (kelch-like family member 40) in 28 apparently unrelated NEM kindreds of various ethnicities. Accounting for up to 28% of the tested individuals in the Japanese cohort, *KLHL40* mutations were found to be the most common cause of this severe form of NEM. Clinical features of affected individuals were severe and distinctive and included fetal akinesia or hypokinesia and contractures, fractures, respiratory failure, and swallowing difficulties at birth. Molecular modeling suggested that the missense substitutions would destabilize the protein. Protein studies showed that KLHL40 is a striated-muscle-specific protein that is absent in *KLHL40*-associated NEM skeletal muscle. In zebrafish, *klhl40a* and *klhl40b* expression is largely confined to the myotome and skeletal muscle, and knockdown of these isoforms results in disruption of muscle structure and loss of movement. We identified *KLHL40* mutations as a frequent cause of severe autosomal-recessive NEM and showed that it plays a key role in muscle development and function. Screening of *KLHL40* should be a priority in individuals who are affected by autosomal-recessive NEM and who present with prenatal symptoms and/or contractures and in all Japanese individuals with severe NEM.

[1]Western Australian Institute for Medical Research and the Centre for Medical Research, University of Western Australia, Nedlands, Western Australia 6009, Australia; [2]Department of Human Genetics, Yokohama City University Graduate School of Medicine, Yokohama 236-0004, Japan; [3]The Folkhälsan Institute of Genetics, Samfundet Folkhälsan, Biomedicum Helsinki, PB 63 (Haartmaninkatu 8), University of Helsinki, Helsinki 00014, Finland; [4]Department of Medical Genetics, Haartman Institute, University of Helsinki, Helsinki 00014, Finland; [5]Department of Neuromuscular Research, National Institute of Neuroscience, National Center of Neurology and Psychiatry, Tokyo 187-8502, Japan; [6]Division of Neurology, Clinical Research Institute, Kanagawa Children's Medical Center, Yokohama 232-8555, Japan; [7]Department of Pediatrics, Odawara Municipal Hospital, Odawara 232-8558, Japan; [8]National Research Institute of Fisheries Science, Yokohama 236-8648, Japan; [9]Department of Biochemistry, Yokohama City University Graduate School of Medicine, Yokohama 236-0004, Japan; [10]School of Biological Sciences, Monash University, Victoria 3800, Australia; [11]The Manton Center for Orphan Disease Research, Genetics and Genomics, Boston Children's Hospital and Harvard Medical School, Boston MA, 02115, USA; [12]Service Génétique Médicale, Hôpital Necker-Enfants Malades, Université Paris Descartes, Paris 75015, France; [13]Unité de Morphologie Neuromusculaire, Institut de Myologie, Institut National de la Santé et de la Recherche Médicale, Paris 75651, France; [14]Lotterywest State Biomedical Facility Genomics and School of Pathology and Laboratory Medicine, University of Western Australia, Perth, Western Australia 6000, Australia; [15]Department of Anatomical Pathology, Royal Perth Hospital, Perth, Western Australia 6000, Australia; [16]Genetic Services of Western Australia, Princess Margaret Hospital for Children and King Edward Memorial Hospital for Women, Subiaco, Western Australia 6008, Australia; [17]Department of Pediatric Neurology, Hacettepe University Children's Hospital, Ankara 06100, Turkey; [18]Department of Pediatric Pathology, Hacettepe University Children's Hospital, Ankara 06100, Turkey; [19]School of Women's and Infants' Health, University of Western Australia, Crawley, Western Australia 6009, Australia; [20]Department of Pathology, University Hospital Antwerp, Antwerp 2650, Belgium; [21]Dubowitz Neuromuscular Centre, UCL Institute of Child Health and Great Ormond Street Hospital for Children, London WC1N 1EH, UK; [22]Institute for Neuroscience and Muscle Research, Children's Hospital at Westmead, Sydney 2145, Australia; [23]Murdoch Childrens Research Institute, The Royal Children's Hospital, Parkville, Victoria 3052, Australia; [24]Unit of Neuromuscular Disorders, Bambino Gesù Children's Hospital, Rome, Lazio 00165, Italy; [25]Neuropediatric Unit, Hadassah Medical Center, Hebrew University of Jerusalem, Jerusalem 91240, Israel; [26]Department of Pediatrics and Pediatric Neurology, University Medicine Göttingen, Göttingen 37075, Germany; [27]Neonatal Intensive Care Unit, Department of Pediatric Research, Women and Children's Division, Oslo University Hospital Rikshospitalet, Oslo 0424, Norway
[28]These authors contributed equally to this work
[29]These authors contributed equally to this work
*Correspondence: nigel.laing@uwa.edu.au (N.G.L.), naomat@yokohama-cu.ac.jp (N.M.)
http://dx.doi.org/10.1016/j.ajhg.2013.05.004.

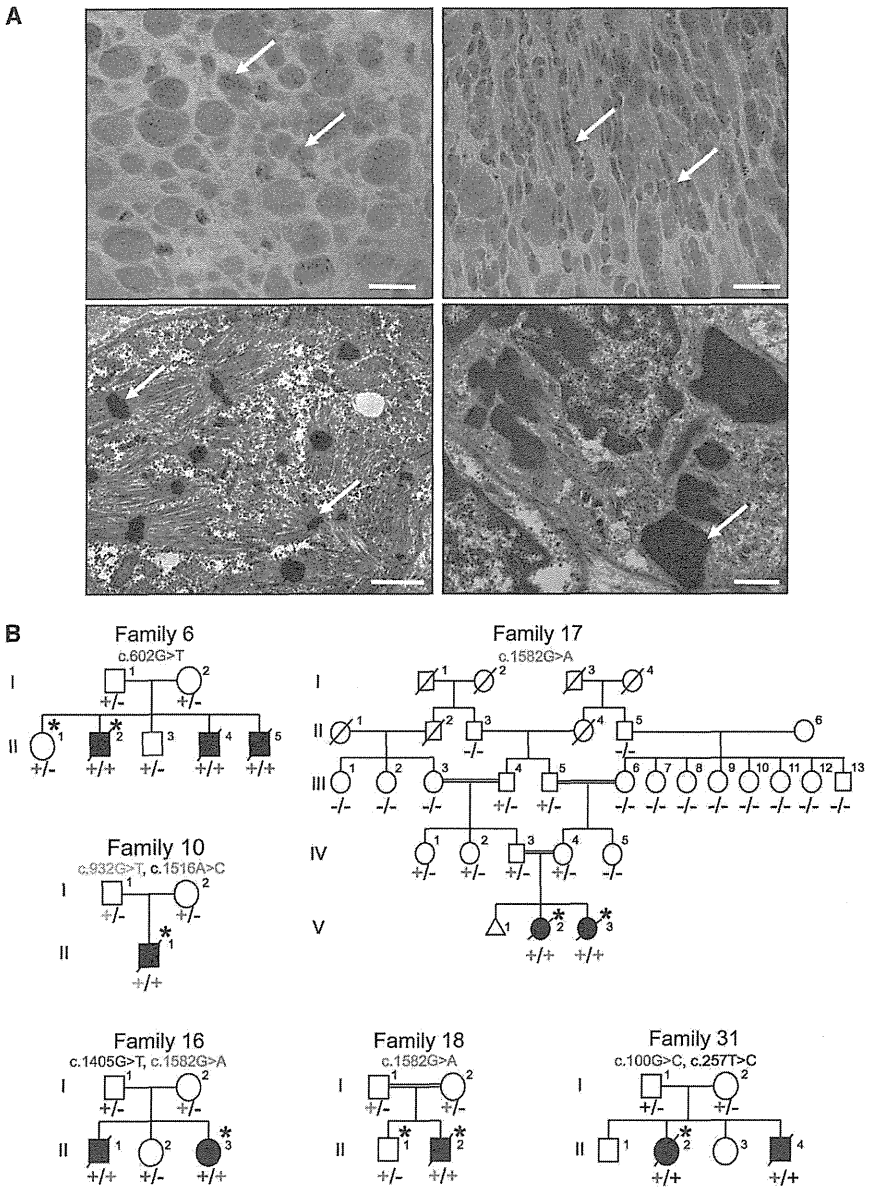

Figure 1. Family Pedigrees and Light and Electron Microscopy of Muscle Biopsies

(A) Modified Gomori trichrome (upper) and electron microscopy (lower) of muscle biopsies from affected individuals of families 15 (right) and 20 (left). Abnormal variation in fiber size, together with many small myofibers and sometimes increased connective tissue, and the presence of numerous red- or purple-stained nemaline bodies (arrows) can be seen (upper panels). Numerous nemaline bodies with varying sizes and shapes and a lack of normal myofibrils are visible by electron microscopy (arrows). Scale bars represent 20 μm for modified Gomori trichrome and 1 μm for electron microscopy.

(B) Pedigrees for the families in which exome sequencing and analysis were performed on the probands. Asterisks indicate the individuals whose DNA was analyzed by exome sequencing. Segregation of the mutations identified in each pedigree is shown.

Introduction

Nemaline myopathy (NEM) is a common form of nondystrophic congenital myopathy and is defined clinically by skeletal-muscle dysfunction and pathologically by the presence of nemaline bodies within myofibers.[1,2] Typical clinical symptoms include hypotonia, muscle weakness of proximal dominance, respiratory insufficiency, and feeding problems. Congenital onset is usual, but a wide variation in age of onset and disease severity is recognized. Mutations in seven genes are known to cause NEM (NEM1–NEM7).[1,2] Six of these encode sarcomere-thin-filament proteins or associated proteins: *ACTA1* (MIM 102610),[3] *CFL2* (MIM 601443),[4] *NEB* (MIM 161650),[5] *TNNT1* (MIM 191041),[6] *TPM2* (MIM 190990),[7] and *TPM3* (MIM 191030);[8] the seventh, *KBTBD13* (kelch-repeat- and BTB-[POZ]-domain-containing 13 [MIM 613727])[9] is involved in the ubiquitin proteasome pathway.[10] Nevertheless, some forms of NEM remain genetically unsolved.

One such subtype, which has long been recognized,[11,12] has apparent autosomal-recessive inheritance and is characterized by severe weakness, in utero presentation of fetal akinesia or hypokinesia and associated abnormalities, and muscle biopsy often showing numerous small nemaline bodies, sometimes only visible by electron microscopy and frequently with virtually no normal myofibrils remaining ("miliary NEM" Figure 1A and Figure S1, available online). We aimed to identify genetic causes of these severe NEM cases by using a combination of linkage analysis, or homozygosity mapping, SNP array, and whole-exome sequencing (WES) in selected families. We have identified loss-of-function mutations in *KLHL40* as a frequent cause of severe NEM and have shown through functional studies that KLHL40 is crucial for myogenesis and skeletal-muscle maintenance.

Subjects and Methods

Subject Details and Ethics

We recruited 143 genetically unresolved severe-NEM-affected families from large congenital-myopathy cohorts in major centers around the world (Boston, Helsinki, Perth, and Tokyo). All individuals within the cohorts were diagnosed with NEM on the basis of muscle-biopsy findings.

Written informed consent was obtained for participation in this study, which was approved by the Human Research Ethics

Committee of the University of Western Australia (UWA), the ethics committee of the Children's Hospital of the University of Helsinki, Yokohama City University School of Medicine, and the Boston Children's Hospital institutional review board. The UWA Animal Ethics Committee approved animal studies.

Microscopy

Light microscopy and electron microscopy of biopsies was performed as previously described.[13]

Whole-Genome SNP Genotyping, Linkage Analysis, and WES

Genotyping was performed for families 6 and 18 with the use of the HumanOmniExpress BeadChip Kit (Illumina) and Infinium II Assay Workflow (Illumina) at the Institute for Molecular Medicine Finland (FIMM). Data were analyzed with PLINK v.1.07. Multiple large homozygous regions were identified, but none included known myopathy-associated genes. WES was performed on one healthy and one affected sibling from family 6 and the proband from family 18 with the SeqCap EZ Human Exome Library v.2.0 exome system (Nimblegen, Roche Diagnostics). Coverage depths were 31- to 62-fold. Variant quantification was performed with the FIMM Variant Calling Pipeline v.1.0 and the Integrative Genomics Viewer (IGV, Broad Institute of MIT and Harvard). All known and heterozygous SNPs were excluded. Healthy siblings' genotypes were used for the exclusion of shared homozygous variants.

Five individuals from family 16 were genotyped with the Human Mapping 10K XbaI 142 2.0 array (Affymetrix) and GeneChip Genotyping Analysis Software (Gtypev4.1). Parametric linkage analysis was performed with Allegro v.2 with a fully penetrant autosomal-recessive model. WES was performed on the proband with the use of the SureSelect Human All Exon 50 Mb Kit (Agilent Technologies) and sequenced in one lane on a GAIIx platform (Illumina) with 108 bp paired-end reads. Reads were aligned to the UCSC Genome Browser (GRCh37/hg19) with Novoalign (Novocraft Technologies). Mean coverage depth was 59-fold. Single-nucleotide variants and small indels were identified with GATK UnifiedGenotyper and filtered according to the Broad Institute's Best Practices guidelines v.3. Variants registered in dbSNP132 were filtered. The filter-passed variants were annotated with ANNOVAR. Only genes with homozygous variants or more than two variants located in the candidate linkage regions were included.

Family 17 was genotyped with the HumanCytoSNP-12 BeadChip (Illumina). MERLIN was used for performing linkage analysis on a subset of 14,514 SNPs.[14] WES was performed for the proband from family 10 and for both siblings from family 17 as described.[15] Coverage depth was 61- to 97-fold. Variants were called with LifeScope 2.5 (Life Technologies) and filtered with ANNOVAR[16] against ENCODE GENCODE v.11 (October 2011 freeze, GRCh37).[17] Two custom variant-filtering steps were used: (1) one against the 1000 Genomes database (February 2012 release) (variants with a minor allele frequency > 0.5% were excluded) and (2) one against the dbSNP135 common database.

Family 31 (BOS74) was one in a cohort of 59 NEM-affected families who underwent WES by the Intellectual and Developmental Disabilities Research Center Core Next-Gen Sequencing Facility of Boston Children's Hospital and Harvard Medical School in collaboration with Axeq Technologies, Complete Genomics, Integrated Genetics (LabCorp), and the Boston Children's Hospital Gene Partnership. Exome sequencing was performed with the Illumina HiSeq 2000 platform. Reads were mapped with the Burrows-Wheeler Aligner (v.0.5.8). SNPs and indels were called with SAMtools (v.0.1.7). Data analysis and variant calling were performed with the Broad GATK Best Practices for identification of SNPs and small indels. Annotated variants were filtered against dbSNP135, the 1000 Genomes Project database (October 2011 edition), and the National Heart, Lung, and Blood Institute (NHLBI) Exome Sequencing Project Exome Variant Server (EVS).

Sequencing

Bidirectional Sanger sequencing of *KLHL40* (RefSeq accession number NM_152393.2) was performed on biobanked DNA from additional probands with severe NEM and their family members in Boston, Helsinki, Perth, Yokohama, and Tokyo. Identified variants were then screened in all available family members. Primer sequences and conditions are available upon request. For detection of the c.1582G>A (p.Glu528Lys) mutation in normal Japanese controls, high-resolution melting (HRM) analysis with and without the spike-in method[18] was performed on LightCycler 480 System II (Roche Diagnostics). If samples showed any aberrant melting patterns, Sanger sequencing was performed for confirmation of the mutation.

LOD Scores

Where possible, MERLIN was used for calculating LOD scores for individual families.[14]

Expression Analysis on Human cDNAs

TaqMan quantitative real-time PCR analyses were performed with cDNAs of human adult (Human MTCPanel I, #636742, Clontech Laboratories) and fetal (Human Fetal MTC Panel, #636747, Clontech Laboratories) tissues.[19] Predesigned TaqMan probe sets for human *KLHL40* (*KBTBD5*, Hs00328078_m1, Applied Biosystems) and human β-actin (*ACTB*, 4326315E, Applied Biosystems) were used. PCR was performed on a Rotor-Gene Q (QIAGEN) (conditions are available upon request) and analyzed with the Rotor-Gene Q Series Software by the $2^{-\Delta\Delta Ct}$ method. Relative concentrations of cDNA were normalized to concentrations obtained from the hearts.

Calculations of the Free-Energy Change upon Amino Acid Substitutions

Molecular structures were drawn with PyMOL. FoldX v.3.0 beta[20] was used through a graphics interface as a plugin for the YASARA molecular viewer.[21] Crystal structures of the kelch domain of human KLHL40 (Protein Data Bank [PDB] code 4ASC) and the BTB (bric-a-brac, tram-track, broad-complex)-BACK (BTB and C-terminal kelch) domain of human KHLH11 (PDB code 3I3N) were energy-minimized with the RepairPDB command implemented in FoldX and subsequently with the BuildModel command for mutagenesis. Protein stabilities were calculated by the Stability command, and the free-energy changes were estimated by subtraction of the free-energy value of the wild-type protein from those of the altered proteins. The procedure was repeated three times for each substitution, and the resultant data were presented as an average value with SDs.

Immunoblotting and Immunohistochemistry

SDS-PAGE and immunoblotting were performed as described.[22,23] For protein studies, C2C12 myoblasts and myotubes were grown and prepared for immunoblotting and immunofluorescence as

described.[23] For KLHL40 immunoblots, the Human Protein Atlas (HPA) rabbit polyclonal KLHL40 (KBTBD5) antibody from Sigma was used (HPA024463 [1:2,500 dilution]). Immunostaining of human and mouse muscle samples was performed as described[13,23] with a KLHL40 antibody (KBTBD5; HPA024463 [1:100 dilution]).

Zebrafish Studies

In Situ Hybridization

Digoxigenin probes for *klhl40a* and *klhl40b* were generated by cDNA amplification of 1,340 and 694 bp sequences, respectively (Table S1). In situ hybridizations were performed as described previously.[24]

Morpholino Microinjection

Antisense translation-blocking morpholinos (Table S1) for *klhl40a* (*klhl40a*-MO) and *klhl40b* (*klhl40b*-MO and *klhl40b*-MO2) were coinjected into 1- to 2-cell-stage embryos at a final concentration of 0.25 or 0.5 mM. Morpholino efficacies were tested by immunoblotting for Klhl40.

Zebrafish Immunohistochemistry

Immunohistochemistry of zebrafish embryos was performed as described[24,25] with myosin heavy chain (MHC) antibody (F59 [1:20 dilution] or A4.1025 [1:10 dilution]; Developmental Studies Hybridoma Bank) and α-actinin (1:100 dilution; Sigma) and filamin C (1:100 dilution; Sigma) antibodies, and Alexa-Fluor-488-conjugated phalloidin (1:100 dilution; Molecular Probes) was used for labeling F-actin. Immunoreactivity was detected with an Alexa-Fluor-594-conjugated anti-mouse secondary antibody diluted in blocking buffer (1:200).

Statistical Analyses

Statistical analyses of clinical features were carried out with SPSS Statistics 19 (IBM) software. Individuals for whom information for a clinical feature was not available were excluded from the analysis of that feature. Either Chi-square tests or Fisher's exact tests were applied for comparing each phenotypic variable between different genotypes. $p < 0.05$ was considered statistically significant.

Results

WES identified homozygous or compound-heterozygous mutations in *KLHL40* (kelch-like family member 40; also known as *KBTBD5* [kelch-repeat- and BTB-(POZ)-domain-containing 5] and *SYRP* [sarcosynapsin]) in six NEM-affected families (families 6, 10, 16–18, and 31; Figure 1B and Table 1). Subsequent screening of *KLHL40* by Sanger sequencing in additional probands with severe NEM resulted in the identification of a total of 19 variants (4 frameshifts, 12 missense mutations, 2 nonsense mutations, and 1 splice site) in 28 (19.6%) apparently unrelated families (Table 1) from the cohort of 143 families affected by severe NEM. In addition, 129 probands with milder NEM were screened, but no *KLHL40* mutations were identified in this cohort, confirming that *KLHL40* mutations are most likely exclusive to cases of severe NEM.

In all cases where it was possible to test unaffected parents, siblings, and extended family, the mutations cosegregated with disease in an autosomal-recessive fashion (Figure 1B), giving a combined LOD score of 5.66 (Table 1). All mutations were either absent from the NHLBI EVS and the 1000 Genomes database[26] or present at low frequencies in the heterozygous state (Table 1). In five additional NEM-affected families, only single *KLHL40* variants were identified (Table S2); the significance of these variants in these individuals remains unclear.

In Japanese persons, *KLHL40* mutations are the most common cause of this severe form of NEM (13/47 [~28%]) as a result of a founder effect with the c.1582G>A mutation. Given that this mutation was present in Turkish, Kurdish, and Japanese families, we completed a haplotype analysis of Japanese and Turkish families (families 16 and 17) but did not identify a common haplotype between them (Figure S2). HRM with confirmatory Sanger sequencing of 510 normal Japanese individuals revealed a heterozygous c.1582G>A mutation in one individual. Therefore, the mutant-allele frequency in the Japanese population was estimated to be 0.0098. According to the equation described by Kimura and Ota[27] and under the assumption of 25 years per generation, the age of this mutation is calculated to be 4,900 years old.

The identified *KLHL40* mutations were scattered throughout all exons (Table 1 and Figure 2A) encoding mostly conserved residues (Figure S3). To investigate disease mechanisms, all substitutions except p.Arg311Leu were mapped to the crystal structures of the kelch domain of human KLHL40 and the BTB-BACK domain of human kelch-like protein 11 (KLHL11; Figures 2B and 2C and Figure S4). p.Arg311Leu (c.932G>T) was predicted to be in the structurally flexible region, a linker of nonconserved amino acids connecting the BACK and kelch domains (Figure S7D), and was therefore excluded from structural consideration. All the modeled substituted residues are involved in intramolecular interactions, and thus the substitutions would most likely destabilize the hydrophobic cores of the BTB-BACK domain (p.Leu86Pro [c.257T>C], p.Val194Glu [c.581T>A], and p.Trp201Leu [c.602G>A]), the kelch domain (p.Pro397Leu [c.1190C>T], p.His455Arg [c.1364A>G], and p.Gly469Cys [c.1405G>T]), the β sheet (p.Thr506Pro [c.1516A>C] and p.Ala538Pro [c.1612G>C]), or the hydrogen bonds between the main chain and side chain (p.Asp34His [c.100G>C] and p.Glu528Lys [c.1582G>A]) or between side chains (p.Glu588Lys [c.1762G>A]) (Figures S5–S7). The p.Pro397Leu and p.Glu588Lys substitutions appear to be conservative for the hydrophobic core and hydrogen bonding, respectively. The former substitution is predicted to affect the polyproline II helix conformation (residues 396–399; Figure S6A). The calculated free-energy change for most substitutions was estimated to be over 2.0 kcal/mol (Figure 2D), which is typically associated with destabilization of domain folds.[28] These analyses suggested that most *KLHL40* missense mutations impair protein stability.

To investigate *KLHL40* expression and KLHL40 abundance, we performed quantitative RT-PCR and immunoblotting of human and mouse tissues. *KLHL40* transcripts

Table 1. ***KLHL40*** **Mutations by Family, Individual LOD Scores, Ethnicity, and Population-wide Incidence**

Family	Exon(s)	Mutation		LOD Score	Ethnicity	Incidence from EVS (1^{st}; 2^{nd})	Incidence from 1000 Genomes (1^{st}; 2^{nd})
		Nucleotide Change	Amino Acid Change				
Family 31[a]	1	c.[100G>C];[257T>C]	p.[Asp34His];[Leu86Pro]	0.6	Vietnamese	ND; ND	ND; ND
Family 2	1	c.[134delC];[134delC]	p.[Pro45Argfs*19];[Pro45Argfs*19]	NA	Italian	NA	ND
Family 3	1	c.[270C>G];[270C>G]	p.[Tyr90*];[Tyr90*]	NA	Turkish	ND	ND
Family 5	1	c.[581T>A];[581T>A]	p.[Val194Glu];[Val194Glu]	0.6	Israeli	ND	ND
Family 6[a]	1	c.[602G>T];[602G>T]	p.[Trp201Leu];[Trp201Leu]	1.454	Turkish	ND	ND
Family 7	1	c.[602G>A];[602G>A]	p.[Trp201*];[Trp201*]	NA	Norwegian	ND	ND
Family 9	1	c.[790delC];[790delC]	p.[Arg264Alafs*59];[Arg264Alafs*59]	0.25	Turkish	NA	ND
Family 10[a]	1 and 4	c.[932G>T];[1516A>C]	p.[Arg311Leu];[Thr506Pro]	NA	Chinese	ND; ND	ND; ND
Family 34	2 and 6	c.[1190C>T];[1762G>A]	p.[Pro397Leu];[Glu588Lys]	NA	Turkish	ND; ND	ND; A = 2 and G = 2,184
Family 12	2 and 4	c.[1270_1272delinsAGATCAAGGT];[1582G>A]	p.[Asp424Argfs*23];[Glu528Lys]	NA	Japanese	NA; ND	ND; ND
Family 13	2 and 4	c.[1281_1294delCTGCCTGGACTCGG];[1582G>A]	p.[Cys428Hisfs*12];[Glu528Lys]	NA	Korean	NA; ND	ND; ND
Family 14	3	c.[1364A>G];[1364A>G]	p.[His455Arg];[His455Arg]	NA	Turkish	ND	ND
Family 15	3	c.[1405G>T];[1405G>T]	p.[Gly469Cys];[Gly469Cys]	NA	Japanese	ND	ND
Family 16[a]	3 and 4	c.[1405G>T];[1582G>A]	p.[Gly469Cys];[Glu528Lys]	0.727	Japanese	ND; ND	ND; ND
Family 17[a]	4	c.[1582G>A];[1582G>A]	p.[Glu528Lys];[Glu528Lys]	1.654	Turkish	ND	ND
Family 18[a]	4	c.[1582G>A];[1582G>A]	p.[Glu528Lys];[Glu528Lys]	0.125	Kurdish	ND	ND
Family 19	4	c.[1582G>A];[1582G>A]	p.[Glu528Lys];[Glu528Lys]	0.25	Kurdish	ND	ND
Family 20	4	c.[1582G>A];[1582G>A]	p.[Glu528Lys];[Glu528Lys]	NA	Japanese	ND	ND
Family 21	4	c.[1582G>A];[1582G>A]	p.[Glu528Lys];[Glu528Lys]	NA	Japanese	ND	ND
Family 22	4	c.[1582G>A];[1582G>A]	p.[Glu528Lys];[Glu528Lys]	NA	Japanese	ND	ND
Family 23	4	c.[1582G>A];[1582G>A]	p.[Glu528Lys];[Glu528Lys]	NA	Japanese	ND	ND
Family 24	4	c.[1582G>A];[1582G>A]	p.[Glu528Lys];[Glu528Lys]	NA	Japanese	ND	ND
Family 25	4	c.[1582G>A];[1582G>A]	p.[Glu528Lys];[Glu528Lys]	NA	Japanese	ND	ND
Family 26	4	c.[1582G>A];[1582G>A]	p.[Glu528Lys];[Glu528Lys]	NA	Japanese	ND	ND
Family 27	4	c.[1582G>A];[1582G>A]	p.[Glu528Lys];[Glu528Lys]	NA	Japanese	ND	ND
Family 28	4	c.[1582G>A];[1582G>A]	p.[Glu528Lys];[Glu528Lys]	NA	Japanese	ND	ND
Family 29	4/5	c.[1608–1G>A];[1608–1G>A]	NA	NA	Turkish	ND	ND
Family 30	5	c.[1612G>C];[1612G>C]	p.[Ala538Pro];[Ala538Pro]	NA	Turkish	ND	ND

The individual pedigree LOD scores are given where possible. This table also shows the incidence of the mutations reported within the NHLBI EVS and the 1000 Genomes browser. Abbreviations are as follows: NA, not available; and ND, not detected.
[a]Families for whom WES was performed.

and their encoded proteins were exclusive to developing and adult skeletal muscle (Figures 3A–3C) and more abundant in fetal muscle than in postnatal muscle (Figure 3C). Confocal microscopy suggested that KLHL40 might localize to the sarcomeric A-band (Figure 3D and Figure S8), a region not previously linked to NEM. Immunoblotting showed that KLHL40 is absent or of low abundance in *KLHL40*-associated NEM muscle (Figure 3E), even for persons harboring two missense mutations (F10 and F17). Immunohistochemistry confirmed that KLHL40 was absent or very scarce in *KLHL40*-associated NEM myofibers (Figure 3F).

We further investigated Klhl40 function in zebrafish. The zebrafish genome contains two orthologs of *KLHL40*: *klhl40a* and *klhl40b*, which have 57% (*klhl40a*) and 55.7% (*klhl40b*) amino acid similarity to human KLHL40. RT-PCR demonstrated expression of both *klhl40* genes at 24 and 48 hr postfertilization (hpf) (Figure S9A). In adult

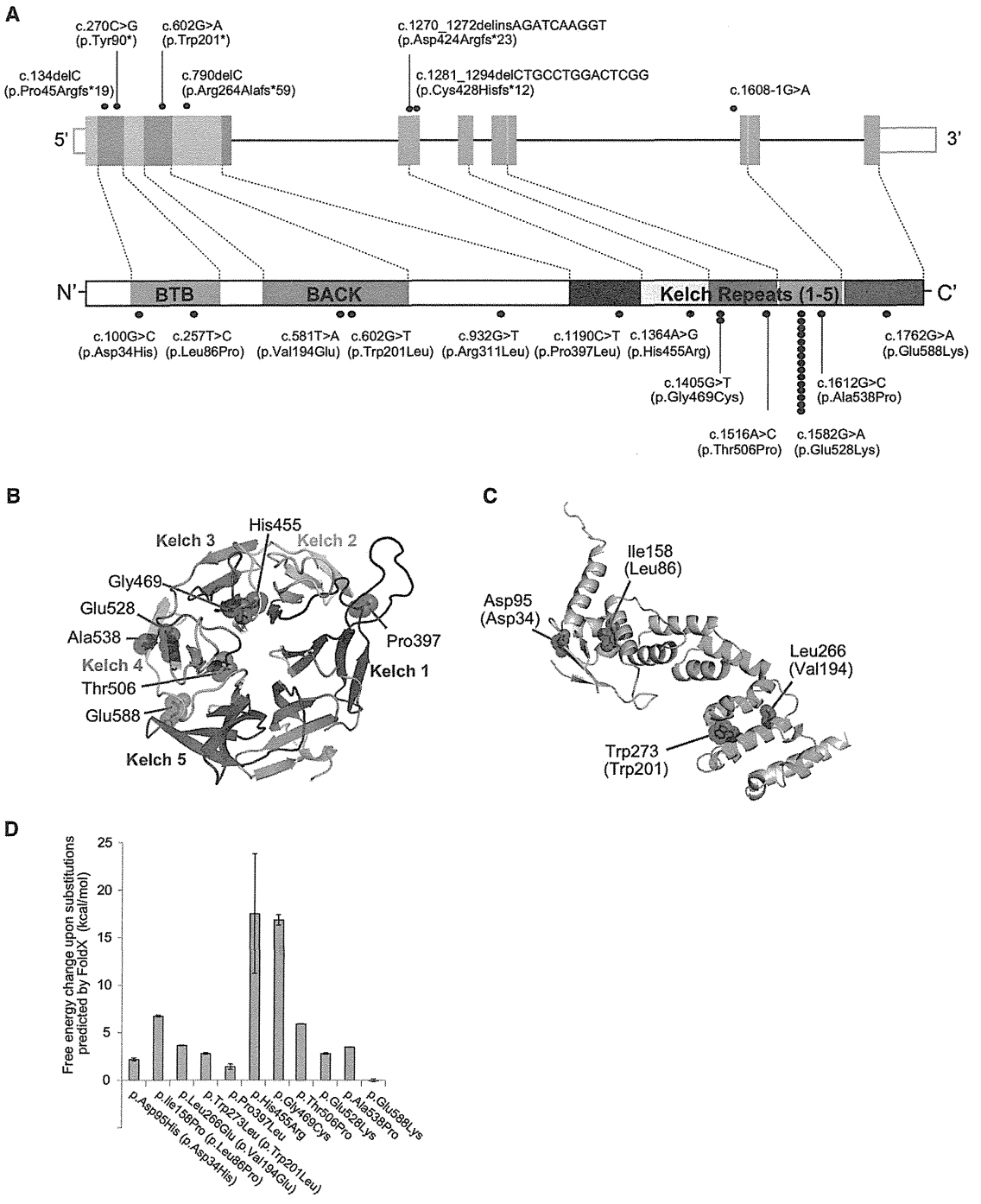

Figure 2. Mutations Identified in Our Cohort and the Structural Modeling of the Missense KLHL40 Substitutions

(A) Schematic presentation of the genomic structure of *KLHL40* (upper) and its encoded protein, KLHL40, with the BTB-BACK domain and kelch repeats (lower). The localization of mutations and substitutions identified is depicted with dots, and the number of dots for each mutation or substitution indicates the number of times it was found. Most substitutions occurred at conserved amino acids. The dots above *KLHL40* indicate truncating mutations, and those below *KLHL40* indicate missense mutations.

(B and C) Structural modeling of the missense KLHL40 substitutions. The crystal structures of the (B) kelch domain of KLHL40 and the (C) BTB-BACK domain of KLHL11 and the location of the substitutions are shown. p.Pro397Leu, p.His455Arg, p.Glu469Cys, p.Thr506Pro, p.Glu528Lys, p.Ala538Pro, and p.Glu588Lys map to the kelch repeats (B), p.Asp34His and p.Leu86Pro map to the BTB domain, and p.Val194Lys and p.Trp201Leu map to the BACK domain (C). The side chains of the mutated residues are shown as sticks with space-filling spheres in red. α helices, β sheets, and loops are drawn as ribbons, arrows, and threads, respectively. Each kelch repeat (B) is color coded in the kelch domain, and the BTB and BACK domains (C) are colored pink and green, respectively. Molecular structures were drawn with PyMOL.

(D) The calculated free-energy changes resulting from the missense substitutions in the kelch domain of human KLHL40 and the BTB-BACK domain of human KLHL11 were predicted by FoldX. Data are presented as the mean ± SD. Residue numbers used in (C) and (D) refer to human KLHL11, and those corresponding to human KLHL40 are in parentheses.

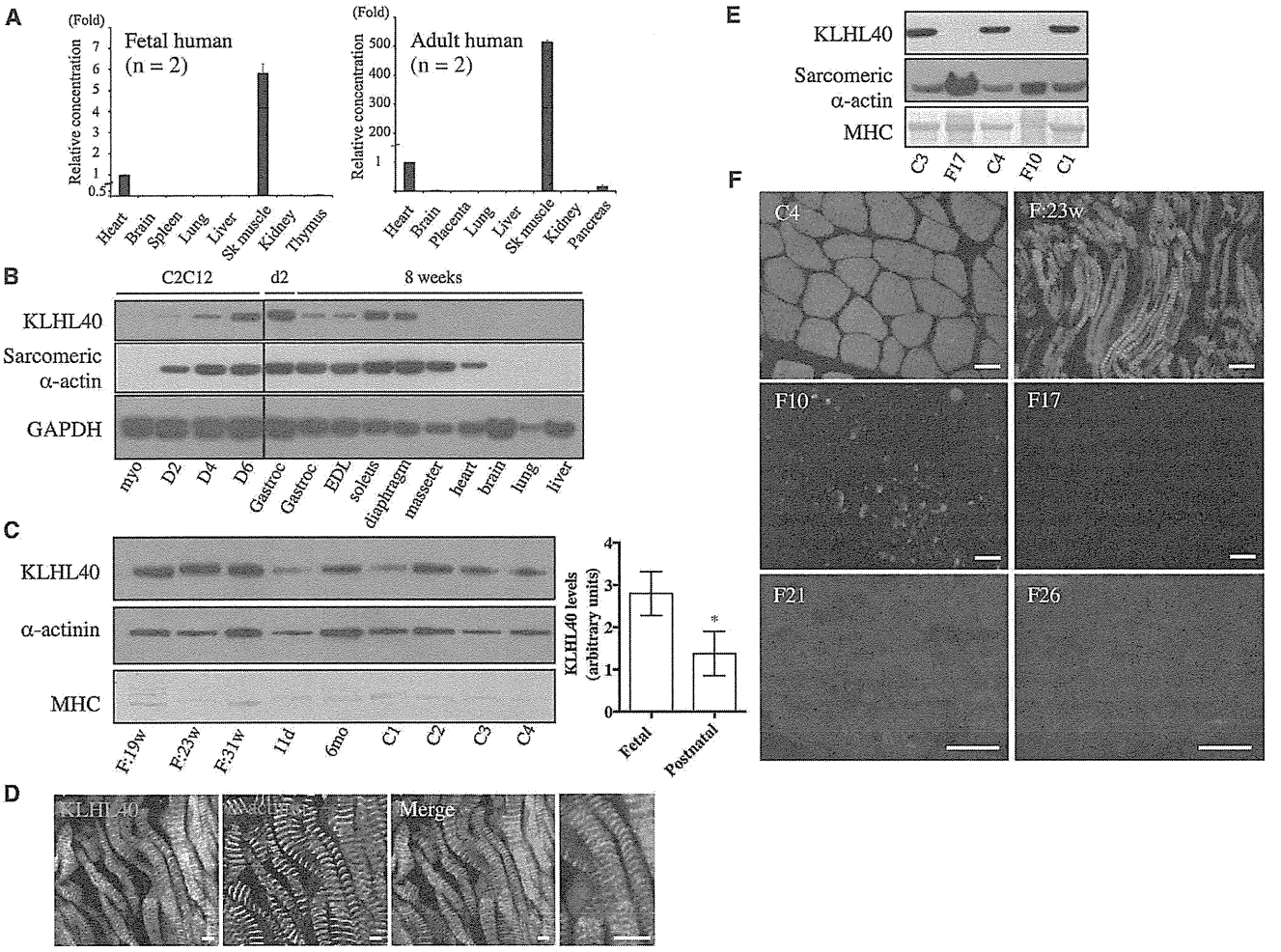

Figure 3. *KLHL40* Expression in Human and Mouse Tissues

(A) Taqman quantitative real-time PCR analysis of cDNA from adult or fetal human tissues. Error bars represent the SD. The following abbreviation is used: Sk, skeletal.

(B) KLHL40 levels in C2C12 cells and mouse tissues (HPA, top panel) and immunoblotting for sarcomeric α-actin (clone 5C5, middle panel) and GAPDH (lower panel). Lanes are as follows: myo, C212 myoblasts; D2, myotubes on day 2 of differentiation; D4, myotubes on day 4 of differentiation; D6, myotubes on day 6 of differentiation; Gastroc (left), C57BL/6 postnatal day 2 (d2) gastrocnemius; Gastroc (right), C57BL/6 8-week-old gastrocnemius; and EDL (extensor digitorum longus) to liver, C57BL/6 8-week-old tissues. For all mouse tissue lysates, samples were pooled from three different mice.

(C) On the left is KLHL40 expression in human skeletal muscle (HPA, top panel), immunoblotting for α-actinin (clone EA-53, middle panel), and Coomassie staining of MHC band (bottom panel). Lanes are as follows: F:19w, 19-week-old fetus; F:23w, 23-week-old fetus; F:31w, 31-week-old fetus; 11d, 11-day-old neonate; 6mo, 6-month-old baby; and C1–C4, healthy adult controls of 19–42 years of age. On the right, KLHL40 intensity normalized to MHC for fetal muscle is 3.34 ± 0.92 (n = 3) versus 1.37 ± 0.21 (n = 6) for postnatal skeletal muscle. *p = 0.023, unpaired two-tailed t test. Error bars represent the SEM.

(D) Single Z-plane confocal microscopy showing localization of KLHL40 (green) and α-actinin (red) in a longitudinal section of skeletal muscle from a 31-week-old fetus; costaining with Hoechst (blue) is also shown (Merge). Scale bars represent 5 μm.

(E) Immunoblotting shows that KLHL40 is absent in *KLHL40*-associated NEM muscle (II-1 from family 10 [F10] and V-2 from family 17 [F17]) compared with healthy control muscle (C1, C3, and C4). Coomassie staining of the MHC band (bottom panel) and immunoblotting for sarcomeric α-actin (clone 5C5, middle panel) indicate similar or greater loading for the *KLHL40*-associated NEM samples compared with control samples.

(F) Immunofluorescence for KLHL40 in a human 23-week-old fetal skeletal muscle sample (F:23w), an adult healthy control (C4), and *KLHL40*-associated NEM muscle biopsies (II-1 from family 10 [F10], V-2 from family 17 [F17], family 21 [F21], and family 26 [F26]). Scale bars represent 50 μm.

zebrafish, *klhl40a* was most abundant in the skeletal muscle and heart and *klhl40b* was most abundant in the skeletal muscle (Figure S9A). At the 16 and 24 hpf stages, expression of both genes was restricted to the muscle precursor cells in the somites (Figure 4A). We knocked down zebrafish *klhl40a* and *klhl40b* with antisense morpholino oligonucleotides (*klhl40a*-MO, *klhl40b*-MO, and *klhl40b*-MO2) (Figures S9B and S10A). Embryos injected with *klhl40a*-MO, *klhl40b*-MO, and *klhl40a*-MO/*40b*-MO (double morpholinos) showed a curved trunk and small head at 48 hpf (Figures 4B and 4C). A normal phenotype resulted from 5 bp mismatched morpholinos (5mis-MOs).

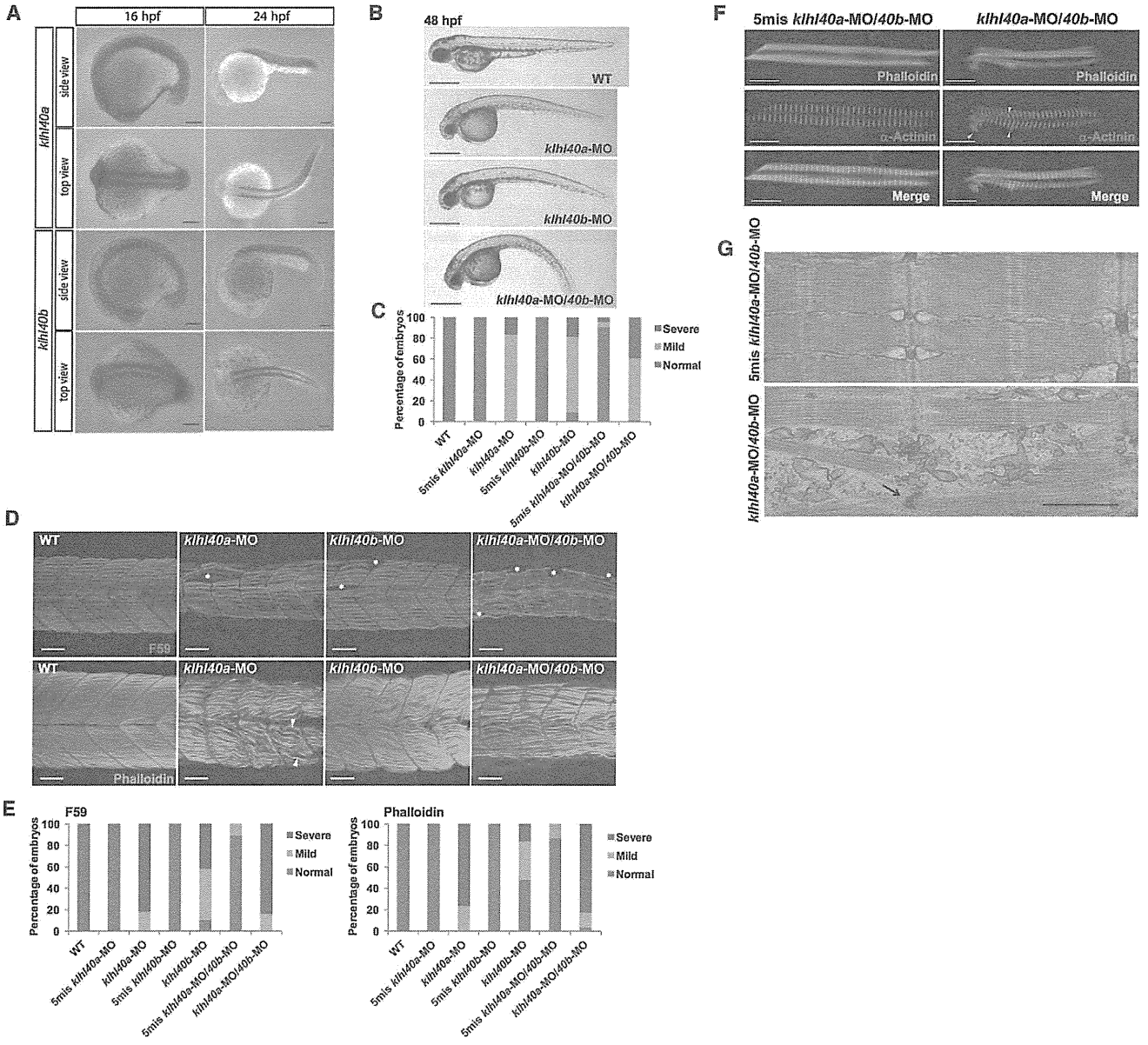

Figure 4. Expression and Function of *klhl40* in Zebrafish

(A) In situ hybridization demonstrates that expression of both *klhl40a* and *klhl40b* is restricted to the skeletal muscle at 16 and 24 hpf.

(B) Gross morphology of uninjected embryos (WT) and embryos injected with *klhl40a*-MO, *klhl40b*-MO, and *klhl40a*-MO/*40b*-MO. Lateral views of MO-injected embryos (4 ng) at 48 hpf are shown. Scale bars represent 500 μm.

(C) Percentage of embryos categorized in phenotypic classes after injection with the 5mis-MO control, *klhl40a*-MO, *klhl40b*-MO, or *klhl40a*-MO/*40b*-MO. We categorized the phenotypes at 48 hpf into normal (normal appearance), mild (curved trunk), and severe (tail defect and severe development delay) (n = 111–130).

(D) Knockdown of *klhl40a*, *klhl40b*, or both resulted in severe disruption of the skeletal muscle: fibers appeared wavy, and there were extensive gaps between fibers in contrast to the densely packed and aligned fibers of the controls. Maximum-intensity projection images from a confocal image series followed immunolabeling with a myosin antibody (F59, upper panels) at 36 hpf and F-actin (lower panels) at 72 hpf.

(E) Embryos injected with 5mis-MO, *klhl40a*-MO, *klhl40b*-MO, or *klhl40a*-MO/*40b*-MO were categorized phenotypically on the basis of the presence of myofiber detachment affecting one to two somites (mild) or multiple (three or more) somites (severe) (n = 25–44).

(F) Double-labeled immunofluorescence was performed on isolated myofibers from 72 hpf embryos with the use of phalloidin (green) and α-actinin (red). Frequent areas of aberrant α-actinin accumulation were detected in *klhl40a*-MO/*40b*-MO myofibers (arrowheads).

(G) Electron microscopy of 72 hpf myofibers. A 5mis-MO-injected embryo shows correctly aligned sarcomeres and T-tubules (upper panel). A *klhl40a*-MO/*40b*-MO-injected embryo (lower panel) shows disarranged myofibrils with widened Z-disks (arrow), but thin filament lengths are unchanged. The scale bar represents 0.7 μm.

We analyzed slow myofibers in more detail by immunostaining slow myosin heavy chains (Figure 4D, upper panels). *klhl40* morphants showed disruption of muscle patterning with an irregular, wavy appearance of the striated myofibers and extensive gaps between the myofibers (Figures 4D and 4E and Figure S10B) and a greatly

Table 2. Summary of Clinical Features of NEM Individuals with *KLHL40* Mutations

	Individuals with *KLHL40* Mutations (n = 32 Cases from 28 Families)	
	Total	**Percentage**
Family history	17/28	60.7%
Consanguinity	10/28	35.7%
Prenatal Period		
Prenatal symptoms	24/29	82.8%
Fetal akinesia or hypokinesia	16/21	76.2%
Polyhydramnios	14/29	48.3%
Neonatal Period		
Respiratory function		
respiratory failure	28/29	96.6%
requiring ventilation	11/29	37.9%
Facial involvement	26/26	100%
weakness	23/23	100%
ophthalmoparesis	4/23	17.4%
mild dysmorphology	15/15	100%
Dysphagia	23/24	95.8%
with tube feeding or gastrostomy	13/24	54.2%
Muscle weakness	29/29	100.0%
with no spontaneous antigravity movements	13/29	44.8%
Contracture(s)	24/27	88.9%
Pathological fracture(s)	10/19	52.6%
Average age at death	5 months (n = 14)	
Average gestation age at birth	37 weeks (n = 27)	
Average birth weight	2,558 g (n = 26)	

Total numbers were calculated as the number of individuals with the clinical features over the total number of individuals whose medical records were available for each category.

diminished birefringence (Figure S10C). Isolated myofibers from *klhl40a*-MO/*40b*-MO fish, coimmunostained with phalloidin and an α-actinin antibody (Z-disk), showed disorganized and irregular patterns with small aggregates of α-actinin, suggesting nemaline bodies (Figure 4F). Aggregation of Z-disk material was also confirmed by immunostaining for filamin C in *klhl40a*-MO/*40b*-MO fish (Figure S11). Electron-microscopic analysis revealed disarranged myofibrils with widened Z-disks (Figure 4G). Fish injected with *klhl40a*-MO, *klhl40b*-MO, *klhl40b*-MO2, or *klhl40a*-MO/*40b*-MO2 (double morpholinos) exhibited sporadic muscle tremors, and coordinated swimming behavior was not observed (Movies S1 and S2). These results suggest that Klhl40a and Klhl40b are required for muscle development and function and that loss of either isoform in the early embryo is sufficient to impair normal mobility.

Detailed clinical records were collected and analyzed for 32 affected individuals from the 28 unrelated kindreds afflicted with *KLHL40* mutations. These individuals were from various ethnicities, such as European, Middle and Near Eastern, or Asian. Clinical features of individuals with *KLHL40* mutations were severe and distinctive (Table 2 and Table S3). Eighty-three percent of affected individuals showed prenatal symptoms, and 76% displayed fetal akinesia or hypokinesia. Most persons had severe respiratory compromise (97%), and approximately a third required ventilatory support (38%). Almost all affected individuals (96%) also had swallowing problems, and half required tube feeding or gastrostomy. Muscle weakness was severe. Forty-five percent of individuals had no spontaneous antigravity movement. Seventeen percent of affected individuals were also noted to have ophthalmoparesis, a relatively rare symptom in NEM. Multiple joint contractures and pathological bone fracture were other common features. Dysmorphic facial features and deformities of the chest, spine, fingers, and feet were also frequent. The average age of death was 5 months. Many families, including a previously described family (family 30 herein, cases 2–6 in Lammens et al.),[11] were consanguineous.

We further evaluated whether there are any genotype-phenotype correlations in *KLHL40*-associated NEM. We compared the clinical features of individuals according to the type of mutation they had (either two truncating mutations, one truncating mutation and one missense mutation, or two missense mutations) and the pattern of mutations (homozygous or compound heterozygous). No significant differences in frequencies of these clinical features were observed (data not shown). We also compared the clinical features of persons with the recurrent c.1582G>A genotype (either with this mutation [genotype G/A or A/A as group A] or without [genotype G/G as group G]). Prenatal symptoms, including fetal akinesia or hypokinesia, were frequently observed (73.3% in group A versus 92.9% in group G). Respiratory failure was common in both groups (100% in group A versus 92.9% in group G), but there were significantly fewer individuals requiring ventilation in group A than in group G (20.0% in group A versus 57.1% in group G; $p = 0.047$). Dysphagia was also common in both groups (100% in group A versus 90.0% in group G), but there were fewer persons requiring tube feeding or gastrostomy in group A than in group G, although the difference was not significant (42.9% in group A versus 70.0% in group G; $p = 0.127$). Facial weakness was observed in all affected individuals in both groups, but fewer individuals in group A had ophthalmoparesis (7.7% in group A versus 30.0% in group G; $p = 0.281$). All persons also had muscle weakness, but significantly fewer individuals in group A had the most severe form of muscle weakness with no antigravity movements (20.0% in group A versus 71.4% in group G; $p = 0.018$). Significantly fewer affected individuals in group A were deceased at the time of study than in group G (23.5% in group A versus 71.4% in group G; $p = 0.012$;